

A localized consensus-based sampling algorithm

Arne Bouillon* Alexander Bodard† Panagiotis Patrinos† Dirk Nuyens*
Giovanni Samaey*

June 2, 2025

Abstract

We develop a novel interacting-particle method for sampling from non-Gaussian distributions. As a first step, we propose a new way to derive the consensus-based sampling (CBS) algorithm, starting from ensemble-preconditioned Langevin diffusions. We approximate the target potential by its Moreau envelope, such that the gradient in the Langevin equation can be replaced by a proximal operator. We then approximate the proximal operator by a weighted mean, and finally assume that the initial and target distributions are Gaussian, resulting in the CBS dynamics. If we keep only those approximations that can be justified in the non-Gaussian setting, the result is a new interacting-particle method for sampling, which we call *localized consensus-based sampling*. We prove that our algorithm is affine-invariant and exact for Gaussian distributions in the mean-field setting. Numerical tests illustrate that localized CBS compares favorably to alternative methods in terms of affine-invariance and performance on non-Gaussian distributions.

Keywords: Consensus-based sampling · Langevin diffusion · Bayesian inverse problems

1 Introduction

We consider the problem of sampling from a probability distribution in d dimensions with density

$$\pi(u) = \frac{\exp(-V(u))}{\int \exp(-V(v)) dv} =: \frac{\hat{\pi}(u)}{Z}, \quad (1)$$

where $V: \mathbb{R}^d \rightarrow \mathbb{R}$ is a potential function with $\int \exp(-V(v)) dv < \infty$. Here, we implicitly take integrals over \mathbb{R}^d . In many applications V is known but the integral Z may be intractable, such that π is available only up to a multiplicative constant.

1.1 Bayesian inverse problems

A common application area to give rise to problem (1) is that of Bayesian inverse problems (see, e.g., [30, 55]). Consider a known model G with unknown parameters u and a perturbed observation

$$y = G(u) + \eta, \quad (2)$$

where η is some unknown measurement noise. The goal is to characterize likely values of u , based on y and G . If we denote by the probability densities $\pi_{\text{prior}}(u)$ and $\pi_{\text{noise}}(\eta)$ our prior

*KU Leuven, Department of Computer Science (NUMA), Celestijnenlaan 200A, 3001 Leuven, Belgium, arne.bouillon@kuleuven.be

†KU Leuven, Department of Electrical Engineering (ESAT-STADIUS), Kasteelpark Arenberg 10, 3001 Leuven, Belgium

beliefs about u and η , then Bayes' rule describes our belief about u after the observation by the *posterior* distribution with density

$$\pi_{\text{post}}(u \mid y) = \frac{\pi_{\text{noise}}(y - G(u)) \pi_{\text{prior}}(u)}{\int \pi_{\text{noise}}(y - G(v)) \pi_{\text{prior}}(v) dv} =: \frac{\hat{\pi}_{\text{post}}(u \mid y)}{\pi_{\text{ev}}(y)}. \quad (3)$$

One approach to solve the Bayesian inverse problem (2) is to find the *maximum a posteriori* (MAP) parameter u_{MAP} that maximizes (3) as discussed in, e.g., [10]:

$$u_{\text{MAP}} := \arg \max_u \hat{\pi}_{\text{post}}(u \mid y). \quad (4)$$

Optimization algorithms can solve the inverse problem in this fashion. However, u_{MAP} gives no information about the uncertainty on u captured by π_{post} . When uncertainty quantification is required, other characteristics of the posterior must be inferred.

In that case, one commonly wants to integrate some function with respect to π_{post} , e.g., to compute statistical moments of the distribution. Numerical integration techniques, such as [25], which uses quasi-Monte Carlo, may provide a sufficient approximation even in high dimensions. Alternatively, it is common to use algorithms that produce a sequence of Monte Carlo samples distributed approximately according to π_{post} . Then solving (2) corresponds to drawing samples from (1), with the *evidence* $\pi_{\text{ev}}(y)$ as the intractable Z and with $\hat{\pi}_{\text{post}}(\cdot \mid y)$ as the unnormalized density $\hat{\pi}$.

1.2 Related literature

Sampling from distributions with density (1) with unknown Z is historically performed with Markov chain Monte Carlo (MCMC) algorithms, which originate in [24, 37] and are reviewed in detail in [3]. MCMC remains a very active research topic with recent developments such as the popular pCN [8] and DILI [9] proposal moves that are effective in high dimensions and multilevel MCMC versions [15, 35] that exploit cheap approximations to G .

An alternative method is sequential Monte Carlo (SMC) [11], which evolves samples from an easy-to-sample distribution (e.g., π_{prior} in (3)) into samples from π (e.g., π_{post}) gradually over multiple (time) steps. Many other methods are based on evolving SDEs that have π (or a distribution approximating π) as an invariant distribution. An example is Langevin diffusion (see subsection 2.1); after time discretization, the unadjusted Langevin algorithm (ULA) [49] arises as an approximate sampler of π . Using ULA steps as MCMC proposals—or, equivalently, adding Metropolis–Hastings rejection to ULA—results in the Metropolis-adjusted Langevin algorithm (MALA) [2].

These Langevin algorithms use derivatives of the potential V , which is often undesirable [16, 32]. McKean–Vlasov-type SDEs (SDEs whose dynamics include their own solution law) discretized with multiple particles have been used to construct various derivative-free (often approximate) samplers. Ensemble Kalman sampling (EKS) [19] and the closely related ALDI method [20] are derived from interacting Langevin diffusions and inspired by the ensemble Kalman inversion (EKI) optimizer [28, 32, 52], which is related to a sequential application of the ensemble Kalman filter (EnKF) [17]. There is also a version of EKI that performs sampling, which is analyzed in [13]. The consensus-based sampling (CBS) method [6], described in more detail in subsection 2.2, was inspired by consensus-based optimization (CBO) [46]. Other samplers based on interacting particles include the multiscale sampler in [43].

Interaction in particle methods can be *localized*: instead of computing a global interaction term, each particle interacts more with particles that are nearby than with those that are far away. The aim of localization is to avoid the linearity assumption on G that is implicit in these methods. Localized algorithms show improved performance for nonlinear G , since the adapted dynamics rely on *local* instead of global linearity. The paper [47] proposed to

use localized interaction in the EKS/ALDI algorithm—details are given in subsection 5.3. Variants on this idea were proposed for EKI and the EnKF [59], for an ensemble Kalman method for rare-event sampling [60], and for CBS as a variant named *polarized CBS* [4]—see subsection 5.2. Our paper develops a different CBS variant with localized interaction, named *localized CBS*.

Remark 1 (Another concept of localization). *We stress that localization as discussed here is unrelated to the notion of localization in [26, 42] for the EnKF, in [1, 58] for EKI, and in [39] for MCMC. There, the empirical covariance matrix is corrected for spurious correlations, caused by a finite ensemble size, between parameter indices that should be uncorrelated—for example, because they correspond to elements at a large distance in the underlying problem. This technique can also increase the rank of the empirical covariance and prevent EKI’s subspace property [58].*

1.3 Objectives and contributions

There are several aspects to consider when assessing sampling algorithms, both computationally and in terms of accuracy.

- (i) *The need for gradients.* Methods that require gradients of V cannot be used when gradients are unavailable.
- (ii) *Parallelizability.* Standard MCMC methods are inherently sequential due to the need to overcome a burn-in phase and are hard to parallelize effectively [54, 61]. Alternatives such as SMC and McKean–Vlasov-based methods use an ensemble of particles in parameter space that exchange information through interaction. This means that any work that is local to a single particle, such as evaluating G , can be trivially parallelized over all particles.
- (iii) *Non-Gaussian performance.* Many sampling methods use approximations that hold only for Gaussian distributions, leading to poor sampling performance on non-Gaussian and multimodal target distributions.
- (iv) *Affine-invariance.* Some algorithms produce poor samples when the different dimensions of π are poorly scaled. The property of affine-invariance (detailed in Definition 2 in the following section) ensures that affine transformations of the parameters do not influence sampling performance.

This paper focuses on gradient-free, parallelizable sampling from poorly scaled, non-Gaussian distributions. We make the following contributions:

- (i) Section 3 proposes a novel way to connect interacting Langevin diffusions [19], which use gradients, to consensus-based sampling (CBS) [6], which does not. This connection is based on three approximations: replacing V by a Moreau envelope, approximating the proximal operator by a weighted mean, and assuming that the initial and target distributions are Gaussian.
- (ii) Subsections 4.1 and 4.2 adapt these approximations, removing those that go against our objective of solving non-Gaussian sampling problems. This results in an algorithm we name *localized consensus-based sampling*. Section 5 compares the existing CBS, polarized CBS, and localized ALDI algorithms to our localized CBS method.

- (iii) We perform an analysis of localized CBS with a broad class of covariance-based preconditioners. We derive ODEs for the evolution of its mean and covariance when applied to Gaussian problems in subsection 4.3. More generally, subsection 4.4 shows that localized CBS is affine-invariant.
- (iv) Section 6 discusses how to efficiently approximate the mean-field equations with finite particle systems, along with other computational considerations. Section 7 performs numerical experiments that showcase the affine-invariance and non-Gaussian performance of localized CBS.

We start our discussion with a brief review of interacting Langevin diffusions and consensus-based sampling in section 2.

1.4 Notation

We define the norm of a vector $v \in \mathbb{R}^n$ weighted by a positive definite matrix $A \in \mathbb{R}^{n \times n}$ as

$$\|v\|_A := \sqrt{v^T A^{-1} v}. \quad (5)$$

Furthermore, we denote by e_i the i th column of an identity matrix and by $\mathbf{1}$ a vector of ones, both of implicit length. The indicator function $\mathbb{1}_S$ takes the value 1 if the condition S is true, and 0 otherwise.

2 Interacting-particle samplers

We now recall the interacting-Langevin and consensus-based samplers, and how they are used to sample in accordance with (1).

2.1 Interacting-Langevin sampling

Let W_t be a standard Brownian motion in \mathbb{R}^d . The Langevin equation reads

$$\dot{U}_t = \nabla \log \hat{\pi}(U_t) + \sqrt{2} \dot{W}_t \quad (6)$$

and, like all SDEs in this paper, should be interpreted in the Itô sense. Preconditioning (6) with a positive definite matrix K can speed up convergence:

$$\dot{U}_t = K \nabla \log \hat{\pi}(U_t) + \sqrt{2K} \dot{W}_t. \quad (7)$$

Denote by ρ_t the law of U_t . Both (6) and (7) have the property that, under certain conditions on $\hat{\pi}$, they transform arbitrary distributions ρ_0 of the initial value U_0 into a distribution $\rho_\infty := \lim_{t \rightarrow \infty} \rho_t$ that is exactly the desired distribution π . This leads to a Monte Carlo algorithm for approximately sampling from π : simulate some number J of discretized paths $\{U_t^j\}_{j=1}^J$ of (6) or (7) until some sufficiently large time T and use $\{U_T^j\}_{j=1}^J$ as the approximate samples.

In [19], the constant matrix K is replaced by a time-varying matrix $\mathcal{C}(\rho_t)$, where ρ_t is the law of U_t and \mathcal{C} denotes the covariance operator. This change results in

$$\dot{U}_t = \mathcal{C}(\rho_t) \nabla \log \hat{\pi}(U_t) + \sqrt{2\mathcal{C}(\rho_t)} \dot{W}_t. \quad (8)$$

The covariance operator \mathcal{C} uses the mean μ in its definition:

$$\mu(\rho) := \int v \, d\rho(v) \quad \text{and} \quad \mathcal{C}(\rho) := \int (v - \mu(\rho)) \otimes (v - \mu(\rho)) \, d\rho(v). \quad (9)$$

Equation (8) is not a special case of (7); rather, it is an extension. The corresponding Fokker–Planck equation is

$$\partial_t \rho_t(u) = \nabla \cdot (\rho_t(u) \mathcal{C}(\rho_t) (-\nabla \log \hat{\pi}(u) + \nabla \log \rho_t(u))). \quad (10)$$

It is shown in [19] that (8) evolves to $\rho_\infty = \pi$ at an exponential rate when V is strongly convex and $\mathcal{C}(\rho_t)$ is bounded from below. In the non-convex case, π is still an invariant distribution. In addition, [20] shows that (8) has the important property of *affine-invariance*.

Definition 2 (Affine-invariance). *Consider an SDE parametrized by the unnormalized target distribution $\hat{\pi}$ (or, equivalently, by the potential V). The SDE is called affine-invariant if it is invariant under affine transformations of the state variables and $\hat{\pi}$. That is, define*

$$\tilde{\pi}(z) = \hat{\pi}(Mz + b) \quad \text{and} \quad \tilde{\rho}_0(z) = |M| \rho_0(Mz + b) \quad (11)$$

for an arbitrary invertible matrix M and vector b . Denote by ρ_t the probability density at time t of solutions to the SDE parameterized by $\hat{\pi}$ and with initial distribution ρ_0 , and by $\tilde{\rho}_t$ the equivalent for $\tilde{\pi}$ and $\tilde{\rho}_0$. Then, the SDE is affine-invariant if

$$\tilde{\rho}_t(z) = |M| \rho_t(Mz + b) \quad \text{for all } t. \quad (12)$$

Similar definitions are found in [20, 34] for SDEs and, earlier, in [22, 23] for discrete-time samplers. The importance of affine-invariance for samplers is widely acknowledged: it guarantees that the sampler will perform as well on poorly scaled distributions as on isotropic distributions. See [22] for an extensive discussion and examples.

Note that the SDE (8) is of McKean–Vlasov type¹: its drift and diffusion coefficients depend on the law ρ_t through $\mathcal{C}(\rho_t)$. It is also possible to use any positive definite preconditioner $\mathbf{C}(\rho_t; U_t)$ that depends on the current position U_t as well as on its law ρ_t . Similarly to what was noted in [40, 47], the resulting SDE

$$\dot{U}_t = \mathbf{C}(\rho_t; U_t) \nabla \log \hat{\pi}(U_t) + \sqrt{2\mathbf{C}(\rho_t; U_t)} \dot{W}_t \quad (13)$$

has as its Fokker–Planck equation

$$\begin{aligned} \partial_t \rho_t(u) &= \nabla \cdot [-\rho_t(u) \mathbf{C}(\rho_t; u) \nabla \log \hat{\pi}(u) + \mathbf{C}(\rho_t; U) \nabla \rho_t(u) + \rho_t(u) \nabla \cdot \mathbf{C}(\rho_t; u)] \\ &= \nabla \cdot [\rho_t(u) \mathbf{C}(\rho_t; u) (-\nabla \log \hat{\pi}(u) + \nabla \log \rho_t(u))] + \nabla \cdot [\rho_t(u) \nabla \cdot \mathbf{C}(\rho_t; u)]. \end{aligned}$$

Without the last term, π would again be invariant under this equation. Hence, one can introduce a correction term into the dynamics to cancel it out; this results in

$$\dot{U}_t = \mathbf{C}(\rho_t; U_t) \nabla \log \hat{\pi}(U_t) + \nabla_u \cdot \mathbf{C}(\rho_t; U_t) + \sqrt{2\mathbf{C}(\rho_t; U_t)} \dot{W}_t. \quad (14)$$

Ideas related to (14) (with an added skew-symmetric matrix in the drift; see also [36]) have been discussed in [34]. Furthermore, (14) underlies the finite-ensemble [40] and localized [47] versions of EKS/ALDI through *statistical linearization* (see [7]).

¹These McKean–Vlasov equations can be simulated by evolving an ensemble of many time-discretized solution paths in parallel and using their empirical distribution instead of the law ρ_t . This is justified by the principle of *propagation of chaos* [56]; for the ensemble Kalman sampler, this was studied in detail in [14]. Until section 6, we study non-discretized McKean–Vlasov SDEs.

2.2 Consensus-based sampling

Consensus-based sampling [6] is defined by the dynamics²

$$\dot{U}_t = -(U_t - \mu_\alpha(\rho_t)) + \sqrt{2(\alpha + 1) \mathcal{C}_\alpha(\rho_t)} \dot{W}_t. \quad (15)$$

Here, $\alpha > 0$ is a method parameter, ρ_t is the law of U_t , and W_t is a standard Brownian motion in \mathbb{R}^d . The weighted mean and covariance μ_α and \mathcal{C}_α are defined as

$$\mu_\alpha(\rho) := \frac{\int v w_\alpha(v) d\rho(v)}{\int w_\alpha(v) d\rho(v)}, \quad (16a)$$

$$\mathcal{C}_\alpha(\rho) := \frac{\int (v - \mu_\alpha(\rho)) \otimes (v - \mu_\alpha(\rho)) w_\alpha(v) d\rho(v)}{\int w_\alpha(v) d\rho(v)}, \quad (16b)$$

where the weight function is given by

$$w_\alpha(v) := \hat{\pi}(v)^\alpha. \quad (17)$$

The SDE (15) is of McKean–Vlasov type, similarly to (14). In [6] it is shown that if ρ_0 and π are Gaussian, then $\lim_{t \rightarrow \infty} \rho_t = \pi$ and the mean and covariance of ρ_t converge exponentially in t . Similarly to interacting Langevin diffusions, CBS is affine-invariant. The mean-field limit of (15) was studied in [21] and [31].

3 Consensus-based sampling as approximate interacting Langevin

We now propose a new connection between interacting-Langevin and consensus-based samplers, arriving at the CBS dynamics (15) starting from (14) by introducing three specific approximations. Throughout the following motivation, we assume that the potential function V is differentiable and L -weakly convex (meaning that $V(\cdot) + \frac{L}{2} \|\cdot\|^2$ is convex for some $L \in \mathbb{R}_0^+$). We also assume that $\mathcal{C}_\alpha(\rho_t)$ is positive definite for all t .

First step: Moreau envelope of V For a positive definite matrix A , denote by

$$V^A(u) := \inf_v (V(v) + \frac{1}{2} \|v - u\|_A^2) \quad (18)$$

the A -Moreau envelope of V . It approximates the potential V , since $V^A(u) \nearrow V(u)$ for all u as $\|A\| \searrow 0$ [50, §1G]. Let us take (14) with $\mathbf{C}(\rho_t; U_t) = \mathcal{C}_\alpha(\rho_t)$ as a starting point. We introduce scalar parameters $\kappa, \gamma > 0$ and approximate V in (14) by its γ -rescaled $\kappa \mathcal{C}_\alpha(\rho_t)$ -Moreau envelope $\gamma V^{\kappa \mathcal{C}_\alpha(\rho_t)}$. We will later choose the parameter γ to counteract the approximation error of the Moreau envelope. If V is L -weakly convex and $\|A\| < L^{-1}$, then V^A has gradient [50, Theorem 2.26]

$$\nabla V^A(u) = (A)^{-1}(u - \mathbf{prox}_V^A(u)), \quad (19)$$

where the *proximal operator* denotes the singleton

$$\mathbf{prox}_V^A(u) := \arg \min_v (V(v) + \frac{1}{2} \|v - u\|_A^2). \quad (20)$$

Note that (19) holds for any positive definite A , regardless of $\|A\|$, if V is convex. By (19), approximating V in (14) by $\gamma V^{\kappa \mathcal{C}_\alpha(\rho_t)}$ allows the gradient-free formulation

$$\dot{U}_t = -\frac{\gamma}{\kappa} \left(U_t - \mathbf{prox}_V^{\kappa \mathcal{C}_\alpha(\rho_t)}(U_t) \right) + \sqrt{2\mathcal{C}_\alpha(\rho_t)} \dot{W}_t. \quad (21)$$

²CBS also has an *optimization mode* where the factor $(\alpha + 1)$ is omitted, which results in an optimization method instead of a sampling one. This paper only considers CBS in sampling mode.

Second step: Weighted mean as approximate proximal operator Solving a minimization problem to evaluate the proximal operator may be expensive. Instead note that the Laplace principle [12, 38] implies (similarly to, e.g., [5])

$$\text{prox}_V^{\kappa\mathcal{C}_\alpha(\rho_t)}(U_t) = \lim_{\beta \rightarrow \infty} \mu_{\beta, \kappa\mathcal{C}_\alpha(\rho_t)/\beta}(\rho_t; U_t) \quad (22)$$

under mild conditions. Here, we used the weighted mean

$$\mu_{a,A}(\rho; u) := \frac{\int v w_{a,A}(v; u) d\rho(v)}{\int w_{a,A}(v; u) d\rho(v)}, \quad (23)$$

$$w_{a,A}(v; u) := \exp(-\|v - u\|_A^2/2) \hat{\pi}(v)^a. \quad (24)$$

The choice $\rho = \rho_t$ in (22) will enable particle approximations in section 7.

Other uses of the proximal operator for Langevin-like sampling include [33, 44, 57]. Related to (22) is the *quantitative Laplace principle* in [18], which was used in conjunction with the proximal operator to study convergence of the consensus-based optimization (CBO) algorithm in [48]. A weighted mean was also used to approximate the proximal operator in [41] in the context of optimization methods. Motivated by (22), we choose some finite $\beta > 0$ and replace the proximal operator by a weighted mean as a second approximation:

$$\dot{U}_t = -\frac{\gamma}{\kappa} \left(U_t - \mu_{\beta, \kappa\mathcal{C}_\alpha(\rho_t)/\beta}(\rho_t; U_t) \right) + \sqrt{2\mathcal{C}_\alpha(\rho_t)} \dot{W}_t. \quad (25)$$

Third step: Gaussian assumption on the target distribution The last step seeks to remove the dependence of the weighted mean on U_t . When ρ_t and π are Gaussian, Appendix A shows that, by choosing the parameters $\kappa = \beta = \alpha$ and $\gamma = 2\alpha/(\alpha + 1)$,

$$\frac{\gamma}{\kappa} (U_t - \mu_{\beta, \kappa\mathcal{C}_\alpha(\rho_t)/\beta}(\rho_t; U_t)) = (\alpha + 1)^{-1} (U_t - \mu_\alpha(\rho_t)). \quad (26)$$

Using this result in the non-Gaussian case as a third approximation results in

$$\dot{U}_t = -(\alpha + 1)^{-1} (U_t - \mu_\alpha(\rho_t)) + \sqrt{2\mathcal{C}_\alpha(\rho_t)} \dot{W}_t. \quad (27)$$

This is simply a time rescaling of the CBS dynamics (15) with a factor $(\alpha + 1)^{-1}$.

4 Localized consensus-based sampling

Armed with the novel interpretation of CBS in section 3, this section derives a new gradient-free sampling method. Our proposed localized consensus-based sampling algorithm retains affine-invariance, is derivative-free, and performs well on non-Gaussian distributions. We study localized CBS in time-continuous, mean-field form; section 6 will then consider discretizations.

4.1 Consensus-based sampling without Gaussian assumption

Recall that our goal is a gradient-free sampling method with good performance on non-Gaussian distributions. We consider the approximations in section 3 that transform interacting Langevin diffusions to CBS, and adapt them to suit this new objective.

The final approximation, from (25) to (27), is only justified for Gaussian π and will be omitted. In addition, we keep the κ and β parameters independent. CBS sets $\kappa = \beta = \alpha$ and compensates this with a suitable γ to still sample from Gaussian distributions exactly, but in the more challenging non-Gaussian case they need to be selected carefully. The Moreau envelope approximation to V suggests that κ should be chosen small, while the weighted-mean

approximation to the proximal operator implies that β should be large. Finally, we note that the steps leading up to (25) are not specific to the preconditioner $\mathcal{C}_\alpha(\rho_t)$ and instead allow a general positive definite preconditioner $\mathbf{C}_t := \mathbf{C}(\rho_t)$. This results in our novel localized CBS dynamics

$$\dot{U}_t = -\frac{\gamma}{\kappa} \left(U_t - \mu_{\beta, \kappa \mathbf{C}_t / \beta}(\rho_t; U_t) \right) + \sqrt{2\mathbf{C}_t} \dot{W}_t. \quad (28)$$

Suitable choices for \mathbf{C}_t include

- (i) a constant matrix $\mathbf{C}_t = K$;
- (ii) an unweighted covariance $\mathbf{C}_t = \mathcal{C}(\rho_t)$; and
- (iii) a weighted covariance $\mathbf{C}_t = \mathcal{C}_\alpha(\rho_t)$, which is used in classical CBS.

The parameter γ could simply be set to 1, but other choices may be able to partially mitigate the bias that is due to $\beta < \infty$ and $\kappa > 0$. We study this bias in more detail in subsection 4.3 as a function of γ , κ , and the choice of \mathbf{C}_t . Notably, when π is Gaussian and \mathbf{C}_t is an unweighted or weighted covariance—choices (ii) and (iii) above—the bias can be removed fully. The value of γ that accomplishes this, given by (38) and (39), can then be used in (28) even in non-Gaussian cases as a heuristic.

4.2 Localized preconditioners

This subsection discusses more general preconditioners for the proposed localized CBS method, at the cost of a correction term and additional computational effort in the resulting algorithm. Concretely, we allow a preconditioner $\mathbf{C}_{U,t} := \mathbf{C}(\rho_t; U_t)$ that depends on the variable U_t as well as its law ρ_t ³. As discussed in subsection 2.1, this requires an additional drift term $\nabla_u \cdot \mathbf{C}_{U,t}$:

$$\dot{U}_t = -\frac{\gamma}{\kappa} \left(U_t - \mu_{\beta, \kappa \mathbf{C}_{U,t} / \beta}(\rho_t; U_t) \right) + \nabla_u \cdot \mathbf{C}_{U,t} + \sqrt{2\mathbf{C}_{U,t}} \dot{W}_t. \quad (29)$$

The corresponding Fokker–Planck equation is

$$\partial_t \rho_t(u) = \nabla \cdot \left(\frac{\gamma}{\kappa} \rho_t(u) (u - \mu_{\beta, \kappa \mathbf{C}_{U,t} / \beta}(\rho_t; u)) + \mathbf{C}_{U,t} \nabla \rho_t(u) \right). \quad (30)$$

A particular choice of interest for the space-dependent preconditioner is

- (iv) a weighted covariance $\mathbf{C}_{U,t} = \mathcal{C}_{\alpha, \lambda \mathcal{C}(\rho_t)}(\rho_t; U_t)$ with scalars $\alpha \geq 0$ and $\lambda > 0$.

Here,

$$\mathcal{C}_{a,A}(\rho; u) := \frac{\int (v - \mu_{a,A}(\rho; u)) \otimes (v - \mu_{a,A}(\rho; u)) w_{a,A}(v; u) \, d\rho(v)}{\int w_{a,A}(v; u) \, d\rho(v)}, \quad (31)$$

which uses the weighted mean (23) and weight function (24). With this preconditioner, the bias of localized CBS can be removed entirely for Gaussian distributions, similarly to the covariances in subsection 4.1, with the γ value given by (40). This weighted covariance is interesting for comparison to the *polarized CBS* method discussed in subsection 5.2, since $\mathcal{C}_{\alpha, \lambda \mathcal{C}(\rho_t)}(\rho; u)$ corresponds to the polarized covariance (54b) with a Gaussian kernel⁴ $k(u, v) = \exp(-(2\lambda)^{-1} \|u - v\|_{\mathcal{C}(\rho_t)}^2)$. Using such a weighted covariance can incur a significant extra computational cost and, in our experiments, does not seem to be needed for good performance of localized CBS.

³When the preconditioner can depend on U_t , a motivation similar to that in section 3 is still possible. In this case, the property (19) gains a quadratic term. As $\|\kappa A\| \rightarrow 0$, this term vanishes, which justifies the use of (19) as an approximation.

⁴Polarized CBS does not include $\mathcal{C}(\rho_t)$ in the distance norm, so the correspondence is not perfect. We add this anisotropy in our covariance weights to ensure affine-invariance (see subsection 4.4).

4.3 Analysis for Gaussian distributions

While the localized CBS dynamics (29) are designed to sample from non-Gaussian distributions, we will now analyze their behavior in detail in the case where the target distribution π is Gaussian, i.e., when $\pi(u) \sim \hat{\pi}(u) = \exp(-V(u)) = \exp(-\frac{1}{2}\|u - m\|_{\Sigma}^2)$ for some m and Σ . This will result in values for γ that we propose to use even in the non-Gaussian case.

Lemma 3. *Assume that the target distribution $\pi = \mathcal{N}(m, \Sigma)$ and the initial condition $U_0 \sim \mathcal{N}(m_0, \Sigma_0)$ are Gaussian. Then, the localized CBS dynamics (29) admit a Gaussian solution $U_t \sim \mathcal{N}(m_t, \Sigma_t)$ with mean and covariance that satisfy*

$$\dot{m}_t = -\frac{\gamma\beta}{\kappa} P_t \Sigma^{-1} (m_t - m), \quad (32a)$$

$$\dot{\Sigma}_t = 2 \left[\mathbf{C}_{*,t} - \frac{\gamma}{\kappa} \Sigma_t + \frac{\gamma\beta}{2\kappa^2} \left(P_t \mathbf{C}_{*,t}^{-1} \Sigma_t + \Sigma_t P_t \mathbf{C}_{*,t}^{-1} \right) \right], \quad (32b)$$

where

$$P_t := \left(\beta \Sigma^{-1} + \Sigma_t^{-1} + \frac{\beta}{\kappa} \mathbf{C}_{*,t}^{-1} \right)^{-1}, \quad (33)$$

if the preconditioner $\mathbf{C}_{*,t} := \mathbf{C}(\rho_t; U_t)$ does not depend on U_t when $\rho_t = \mathcal{N}(m_t, \Sigma_t)$. This is the case, for example, for the preconditioners considered before:

$$\mathbf{C}(\rho_t; U_t) = K, \quad (34a)$$

$$\mathbf{C}(\rho_t; U_t) = \mathcal{C}(\rho_t) = \Sigma_t, \quad (34b)$$

$$\mathbf{C}(\rho_t; U_t) = \mathcal{C}_{\alpha}(\rho_t) = (\alpha \Sigma^{-1} + \Sigma_t^{-1})^{-1}, \quad (34c)$$

$$\mathbf{C}(\rho_t; U_t) = \mathcal{C}_{\alpha, \lambda \mathcal{C}(\rho_t)}(\rho_t; U_t) = (\alpha \Sigma^{-1} + (1 + \lambda^{-1}) \Sigma_t^{-1})^{-1}. \quad (34d)$$

Proof. Assume that $\rho_t = \mathcal{N}(m_t, \Sigma_t)$. From the condition that $\mathbf{C}_{*,t}$ not depend on U_t follows $\nabla_u \cdot \mathbf{C}_{*,t} = 0$. Similarly to [4], in Appendix A we derive the rightmost terms in (34b)–(34d) and

$$\mu_{\beta, \kappa \mathbf{C}_{*,t}/\beta}(\rho_t; U_t) = (\beta \Sigma^{-1} + \Sigma_t^{-1} + \frac{\beta}{\kappa} \mathbf{C}_{*,t}^{-1})^{-1} (\beta \Sigma^{-1} m + \Sigma_t^{-1} m_t + \frac{\beta}{\kappa} \mathbf{C}_{*,t}^{-1} U_t). \quad (35)$$

In this case, (29) becomes a *linear SDE*: the drift term depends on U_t in an affine way and the diffusion term is U_t -independent. Following, e.g., [51, Section 6.1], the SDE admits a Gaussian solution with mean and covariance that satisfy

$$\begin{aligned} \dot{m}_t &= -\frac{\gamma}{\kappa} \left(I - \frac{\beta}{\kappa} P_t \mathbf{C}_{*,t}^{-1} \right) m_t + \frac{\gamma}{\kappa} P_t (\beta \Sigma^{-1} m + \Sigma_t^{-1} m_t), \\ &= -\frac{\gamma}{\kappa} \left[\left(I - P_t (P_t^{-1} - \beta \Sigma^{-1}) \right) m_t - P_t \beta \Sigma^{-1} m \right] = -\frac{\gamma\beta}{\kappa} P_t \Sigma^{-1} (m_t - m) \end{aligned} \quad (36)$$

and

$$\dot{\Sigma}_t = -\frac{\gamma}{\kappa} \left(I - \frac{\beta}{\kappa} P_t \mathbf{C}_{*,t}^{-1} \right) \Sigma_t - \frac{\gamma}{\kappa} \Sigma_t \left(I - \frac{\beta}{\kappa} P_t \mathbf{C}_{*,t}^{-1} \right) + 2 \mathbf{C}_{*,t}, \quad (37)$$

which simplifies into (32b). \square

Corollary 4. *Assume that the target distribution $\pi = \mathcal{N}(m, \Sigma)$ is Gaussian. The localized CBS dynamics admit π as a stationary distribution in the following cases.*

(i) *The preconditioner is the unweighted covariance $\mathbf{C}_{U,t} = \mathcal{C}(\rho_t)$ and*

$$\gamma = \kappa + \frac{\beta}{\beta + 1}. \quad (38)$$

(ii) The preconditioner is the weighted covariance $\mathbf{C}_{U,t} = \mathcal{C}_\alpha(\rho_t)$ and

$$\gamma = (\alpha + 1)^{-1} \kappa + \frac{\beta}{\beta + 1}. \quad (39)$$

(iii) The preconditioner is the weighted covariance $\mathbf{C}_{U,t} = \mathcal{C}_{\alpha, \lambda \mathcal{C}(\rho_t)}(\rho_t; U_t)$ and

$$\gamma = \left(\frac{1}{\lambda} + \alpha + 1 \right)^{-1} \kappa + \frac{\beta}{\beta + 1}. \quad (40)$$

Proof. For π to be a stationary distribution of localized CBS, we need $\partial_t \rho_t(u) = 0$ when $\rho_t = \pi$. Since then both ρ_t and π are Gaussian, we can use Lemma 3, fill in an expression for the preconditioner such as (34), and require $\dot{m}_t = 0$ and $\dot{\Sigma}_t = 0$ when $m_t = m$ and $\Sigma_t = \Sigma$. Clearly, \dot{m}_t as given by (32a) is zero irrespective of γ and $\mathbf{C}_{*,t}$ when $m_t = m$. For $\dot{\Sigma}_t$, we have

$$\dot{\Sigma}_t = 2 \left[\mathbf{C}_{*,t} - \frac{\gamma}{\kappa} \Sigma + \frac{\gamma \beta}{2 \kappa^2} \left(P_t \mathbf{C}_{*,t}^{-1} \Sigma + \Sigma P_t \mathbf{C}_{*,t}^{-1} \right) \right]. \quad (41)$$

When $\mathbf{C}_{*,t}$ and $\Sigma_t = \Sigma$ commute—which is the case for the three preconditioners considered in this corollary, as seen in (34)—we can simplify (41) to

$$\begin{aligned} \dot{\Sigma}_t &= 2 \left[\mathbf{C}_{*,t} + \frac{\gamma}{\kappa} \left(\left(\kappa \frac{\beta + 1}{\beta} \mathbf{C}_{*,t} \Sigma^{-1} + I \right)^{-1} - I \right) \Sigma \right] \\ &= 2 \left[\mathbf{C}_{*,t} - \frac{\gamma}{\kappa} \left(\kappa \frac{\beta + 1}{\beta} \mathbf{C}_{*,t} \Sigma^{-1} + I \right)^{-1} \left(\kappa \frac{\beta + 1}{\beta} \mathbf{C}_{*,t} \Sigma^{-1} \right) \Sigma \right] \\ &= 2 \left[\mathbf{C}_{*,t} - \gamma \left(\kappa \Sigma^{-1} + \frac{\beta}{\beta + 1} \mathbf{C}_{*,t}^{-1} \right)^{-1} \right], \end{aligned} \quad (42)$$

which, after some algebraic manipulations, can be seen to equal zero when

$$\kappa I = \left(\gamma - \frac{\beta}{\beta + 1} \right) \Sigma \mathbf{C}_{*,t}^{-1}. \quad (43)$$

For the weighted covariance, (34d) becomes $\mathbf{C}_{*,t} = (\lambda^{-1} + \alpha + 1) \Sigma$ when $\Sigma_t = \Sigma$, which means that (43) is satisfied when γ is given by (40). The other cases correspond to specific choices for λ and α and are analogous. \square

A statement such as Corollary 4 about the preconditioner $\mathbf{C}_{*,t} = K$ is not possible, since there does not exist a γ for which (41) is satisfied for all Σ in this case.

4.4 Affine-invariance

We now study affine-invariance of localized CBS.

Lemma 5. *The SDE (29) is affine-invariant when the preconditioner is given by $\mathbf{C}(\rho_t; U_t) = \mathcal{C}(\rho_t)$, $\mathbf{C}(\rho_t; U_t) = \mathcal{C}_\alpha(\rho_t)$, or $\mathbf{C}(\rho_t; U_t) = \mathcal{C}_{\alpha, \lambda \mathcal{C}(\rho_t)}(\rho_t; U_t)$.*

Proof. To prove affine-invariance following Definition 2, we use the Fokker–Planck equation (30) and make the dependence on $\hat{\pi}$ explicit:

$$\partial_t \rho_t(u) = \nabla \cdot \left(\frac{\gamma}{\kappa} \rho_t(u) \left(u - \mu_{\beta, \kappa \mathbf{C}^{\hat{\pi}}(\rho_t; u)/\beta}^{\hat{\pi}}(\rho_t; u) \right) + \mathbf{C}^{\hat{\pi}}(\rho_t; u) \nabla \rho_t(u) \right). \quad (44)$$

With the transformed $\tilde{\pi}(z) = \hat{\pi}(Mz + b)$, the Fokker–Planck equation looks like

$$\partial_t \tilde{\rho}_t(z) = \nabla \cdot \left(\frac{\gamma}{\kappa} \tilde{\rho}_t(z) \left(z - \mu_{\beta, \kappa \mathbf{C}^{\tilde{\pi}}(\tilde{\rho}_t; z)/\beta}^{\tilde{\pi}}(\tilde{\rho}_t; z) \right) + \mathbf{C}^{\tilde{\pi}}(\tilde{\rho}_t; z) \nabla \tilde{\rho}_t(z) \right). \quad (45)$$

Now define

$$\bar{\rho}_t(z) = |M| \rho_t(Mz + b); \quad (46)$$

then, by Definition 2, localized CBS is affine-invariant if (45) holds for $\tilde{\rho}_t = \bar{\rho}_t$. As a first step, one can check that these preconditioners satisfy (with $u = Mz + b$)

$$\mathbf{C}^{\hat{\pi}}(\rho_t; u) = M \mathbf{C}^{\tilde{\pi}}(\bar{\rho}_t; z) M^T \quad (47)$$

and, thus, that

$$\mu_{\beta, \kappa \mathbf{C}^{\hat{\pi}}(\rho_t; u)}^{\hat{\pi}}(\rho_t; u) = M \mu_{\beta, \kappa \mathbf{C}^{\tilde{\pi}}(\bar{\rho}_t; z)}^{\tilde{\pi}}(\bar{\rho}_t; z) + b. \quad (48)$$

We can then write

$$\begin{aligned} \partial_t \bar{\rho}_t(z) &= |M| \partial_t \rho_t(u) \\ &= |M| \nabla_u \cdot \left(\frac{\gamma}{\kappa} \rho_t(u) (u - \mu_{\beta, \kappa \mathbf{C}^{\hat{\pi}}(\rho_t; u)}^{\hat{\pi}}(\rho_t; u)) + \mathbf{C}^{\hat{\pi}}(\rho_t; u) \nabla_u \rho_t(u) \right) \\ &= \nabla_u \cdot \left(\frac{\gamma}{\kappa} M \bar{\rho}_t(z) (z - \mu_{\beta, \kappa \mathbf{C}^{\tilde{\pi}}(\bar{\rho}_t; z)}^{\tilde{\pi}}(\bar{\rho}_t; z)) + M \mathbf{C}^{\tilde{\pi}}(\bar{\rho}_t; z) \nabla_z \bar{\rho}_t(z) \right) \\ &= \nabla_z \cdot \left(\frac{\gamma}{\kappa} \bar{\rho}_t(z) (z - \mu_{\beta, \kappa \mathbf{C}^{\tilde{\pi}}(\bar{\rho}_t; z)}^{\tilde{\pi}}(\bar{\rho}_t; z)) + \mathbf{C}^{\tilde{\pi}}(\bar{\rho}_t; z) \nabla_z \bar{\rho}_t(z) \right). \end{aligned}$$

This proves affine-invariance. \square

5 Comparison to alternative methods

This section compares the dynamics (29) of localized CBS to those of various other McKean–Vlasov-based samplers. A detailed numerical comparison follows in section 7; here, we focus on different aspects of the dynamics and how these may affect the properties of the resulting algorithms.

5.1 Consensus-based sampling

We derived localized CBS in section 4 as a generalization of classical CBS to non-Gaussian sampling problems. We will now show that, when both the target distribution π and the initial particle distribution ρ_0 are Gaussian, the localized CBS dynamics (29) with a certain weighted covariance as preconditioner admit the same solution as the CBS dynamics (15).

Lemma 6. *Let $U_t \sim \mathcal{N}(m_t, \Sigma_t)$ follow the localized CBS dynamics (29) preconditioned with the weighted covariance $\mathbf{C}(\rho; u) = \mathcal{C}_{\alpha, \lambda \mathcal{C}(\rho)}(\rho; u)$ and let $U'_t \sim \mathcal{N}(m'_t, \Sigma'_t)$ follow the CBS dynamics (15). The target density $\pi = \mathcal{N}(m, \Sigma)$ and initial densities $\mathcal{N}(m_0, \Sigma_0) = \mathcal{N}(m'_0, \Sigma'_0)$ are Gaussian.*

For any choice of the CBS parameter⁵ $\alpha' > 0$ and with localized CBS parameters

$$\alpha > 0, \quad \kappa = \alpha, \quad \beta = \alpha', \quad \text{and} \quad \lambda = \frac{\alpha'}{\alpha - \alpha'}, \quad (49)$$

it holds that $m_t = m'_{ct}$ and $\Sigma_t = \Sigma'_{ct}$ with

$$c = \frac{\alpha'}{\alpha(\alpha' + 1)}. \quad (50)$$

⁵We write α' for the CBS parameter to distinguish it from the α parameter of localized CBS.

Proof. In [6], it is shown that

$$\dot{\Sigma}'_t = -2\alpha'\Sigma'_t(\Sigma + \alpha'\Sigma'_t)^{-1}(\Sigma'_t - \Sigma). \quad (51)$$

On the other hand, filling in (49) into (32b) with (34d) results in

$$\begin{aligned} \dot{\Sigma}_t &= 2 \left[\mathbf{C} - 2 \frac{\alpha'}{\alpha(\alpha' + 1)} \Sigma_t + \frac{(\alpha')^2}{\alpha^2(\alpha' + 1)} \left(P_t \mathbf{C}^{-1} \Sigma_t + \Sigma_t P_t \mathbf{C}^{-1} \right) \right] \\ &= 2 \left[\mathbf{C} - 2c\Sigma_t + c \frac{\alpha'}{\alpha} \left(\frac{\alpha}{\alpha'} I \Sigma_t + \Sigma_t \frac{\alpha}{\alpha'} I \right) \right] \\ &= 2 \left[\left(\alpha \Sigma^{-1} + \frac{\alpha}{\alpha'} \Sigma_t^{-1} \right)^{-1} - c\Sigma_t \right] \\ &= 2 \left[c(\Sigma_t - \alpha'\Sigma_t(\Sigma + \alpha'\Sigma_t)^{-1}(\Sigma_t - \Sigma)) - c\Sigma_t \right] \\ &= 2c\alpha'\Sigma_t(\Sigma + \alpha'\Sigma_t)^{-1}(\Sigma_t - \Sigma), \end{aligned}$$

where we noted that $\gamma = 2\frac{\alpha'}{\alpha'+1}$. This is the same ODE as (51), but accelerated with a factor c ; hence, $\Sigma_t = \Sigma'_{ct}$.

Again from [6], we obtain

$$\dot{m}'_t = -\alpha'\Sigma'_t(\Sigma + \alpha'\Sigma'_t)^{-1}(m'_t - m). \quad (52)$$

For localized CBS, (32a) becomes

$$\begin{aligned} \dot{m}_t &= -2\alpha'cP_t\Sigma^{-1}(m_t - m) = -c\alpha'\Sigma_t(\Sigma + \alpha'\Sigma_t)^{-1}(m_t - m) \\ &= -c\alpha'\Sigma'_{ct}(\Sigma + \alpha'\Sigma'_{ct})^{-1}(m_t - m). \end{aligned}$$

This is the ODE (52) accelerated with a factor c . We conclude that $m_t = m'_{ct}$. \square

For non-Gaussian distributions, this configuration of localized CBS likely performs quite poorly due to the large κ value. Lemma 6 is mainly of theoretical interest as a generalization of our argument in section 3 to space-dependent preconditioners.

5.2 Polarized consensus-based sampling

A recently proposed modification of CBS, called polarized CBS [4], makes the weight function dependent on the position U_t through a *polarization kernel* $k(\cdot, \cdot)$. This results in the dynamics

$$\dot{U}_t = -(U_t - \tilde{\mu}_{\alpha,k}(\rho_t; U_t)) + \sqrt{2(\alpha + 1)\tilde{\mathcal{C}}_{\alpha,k}(\rho_t; U_t)} \dot{W}_t, \quad (53)$$

with the polarized mean and covariance

$$\tilde{\mu}_{\alpha,k}(\rho; u) := \frac{\int v \tilde{w}_{\alpha,k}(v; u) d\rho(v)}{\int \tilde{w}_{\alpha,k}(v; u) d\rho(v)}, \quad (54a)$$

$$\tilde{\mathcal{C}}_{\alpha,k}(\rho; u) := \frac{\int (v - \tilde{\mu}_{\alpha,k}(\rho; u)) \otimes (v - \tilde{\mu}_{\alpha,k}(\rho; u)) \tilde{w}_{\alpha,k}(v; u) d\rho(v)}{\int \tilde{w}_{\alpha,k}(v; u) d\rho(v)}, \quad (54b)$$

where

$$\tilde{w}_{\alpha,k}(v; u) = k(v, u) \hat{\pi}(v)^\alpha. \quad (55)$$

The main kernel used in [4] is Gaussian: for positive definite matrix D and scalar λ ,

$$k(v, u) = \exp\left(-(2\lambda)^{-1}\|v - u\|_D^2\right). \quad (56)$$

This choice of k introduces a localization effect: the polarized mean $\tilde{\mu}_{\alpha,k}(\rho_t; U_t)$ —the “target” of the drift in (53)—tends to produce a value that is close to U , as well as having a large density in the posterior $\pi \propto \hat{\pi}$. When π is Gaussian, [4, Proposition 1] proves that π is a stationary distribution of (53) with (56). More generally, a localized kernel attempts to lessen the Gaussian assumption present in CBS.

Equation (53) is very reminiscent of the localized CBS dynamics (29). We now compare the two, highlighting three main differences.

- (i) Localized CBS includes the correction term $\nabla_u \cdot \mathbf{C}_{U,t}$. As $\beta \rightarrow \infty$ and $\kappa \rightarrow 0$, then, we expect convergence to the corrected interacting Langevin dynamics, under which even non-Gaussian and multimodal π are invariant. In polarized CBS, we do not expect a similar convergence.
- (ii) By including the preconditioner $\mathbf{C}_{U,t}$ in the distance weighting for the localized mean, localized CBS has affine-invariant dynamics when $\mathbf{C}_{U,t}$ is a weighted or unweighted covariance. The polarization kernels proposed for polarized CBS in [4], on the other hand, are not affine-invariant.
- (iii) Using $\hat{\pi}$ -based and distance-based weights in the (relatively cheap) mean computation is crucial in both methods, since that drives evolution towards high-probability regions and allows multimodal sampling. On the other hand, we find that the benefits of using weights in the (relatively expensive) covariance preconditioner are significantly less clear. Yet, this can be costly: distance-weighted statistics need to be computed for each of the J particles, instead of once, globally. Polarized CBS uses the same weighting for both the mean and the covariance, while localized CBS decouples these two elements and allows to use a cheap, unweighted covariance as a preconditioner. Especially in higher-dimensional problems, this can make localized CBS the computationally cheaper method.

5.3 Localized ALDI

The gradient-free McKean–Vlasov dynamics underlying the closely related EKS and ALDI algorithms [19, 20] are described by

$$\dot{U}_t = -\mathcal{C}^G(\rho_t)\Gamma^{-1}(G(U_t) - y) + \mathcal{C}(\rho_t)\Gamma_0^{-1}(U_t - u_0) + \sqrt{2\mathcal{C}(\rho_t)}\dot{W}_t, \quad (57)$$

where

$$\mu^G(\rho) := \int G(v) d\rho(v) \quad \text{and} \quad \mathcal{C}^G(\rho) := \int (v - \mu(\rho)) \otimes (G(v) - \mu^G(\rho)) d\rho(v). \quad (58)$$

Equation (57) approaches the sampling problem (1) explicitly in the context of a Bayesian inverse problem (2), estimating the parameters of a forward model G . It also assumes that $\pi_{\text{prior}} = \mathcal{N}(u_0, \Gamma_0)$ and $\pi_{\text{noise}} = \mathcal{N}(0, \Gamma)$ are Gaussians. In the case where G is linear, (57) is equivalent to (8) and, hence, has π as an invariant distribution [19]. For nonlinear G , this is generally not the case.

In [47], localization with a scalar λ and positive definite matrix D is added to (57), together with a correction term similar to the one in (14). This results in

$$\begin{aligned} \dot{U}_t = & -\tilde{\mathcal{C}}_{\lambda D}^G(\rho_t; U_t)\Gamma^{-1}(G(U_t) - y) - \tilde{\mathcal{C}}_{\lambda D}(\rho_t; U_t)\Gamma_0^{-1}(U_t - u_0) \\ & + \nabla_u \cdot \tilde{\mathcal{C}}_{\lambda D}(\rho_t; U_t) + \sqrt{2\tilde{\mathcal{C}}_{\lambda D}(\rho_t; U_t)}\dot{W}_t, \end{aligned} \quad (59)$$

where

$$\tilde{\mu}_{\lambda D}(\rho; u) := \frac{\int v \tilde{w}_{\lambda D}(v; u) d\rho(v)}{\int \tilde{w}_{\lambda D}(v; u) d\rho(v)}, \quad (60a)$$

$$\tilde{\mathcal{C}}_{\lambda D}(\rho; u) := \frac{\int (v - \tilde{\mu}_{\lambda D}(\rho; u)) \otimes (v - \tilde{\mu}_{\lambda D}(\rho; u)) \tilde{w}_{\lambda D}(v; u) d\rho(v)}{\int \tilde{w}_{\lambda D}(v; u) d\rho(v)} \quad (60b)$$

with

$$\tilde{w}_{\lambda D}(v; u) = \exp(-(2\lambda)^{-1} \|v - u\|_D^2). \quad (61)$$

The definition of $\tilde{\mathcal{C}}_{\lambda D}^G$ is analogous. We stress again that this is a different concept of localization than the one discussed in Remark 1.

This localization improves performance for nonlinear G , making localized ALDI a viable method for our problem class. However, we point out two potential advantages of the localized CBS dynamics.

- (i) Similarly to polarized CBS, when the matrix D in the distance-based weights of localized ALDI is fixed, the dynamics are not affine-invariant. In [47], affine-invariance is proven if $D = \mathcal{C}(\rho_0)$, such that D is also subject to any affine transformation. This can be considered a slightly weaker form of affine-invariance: in practice, the scaling of the parameters is often not fully known and ρ_0 cannot be chosen with optimal scaling. After all, if the scaling was known exactly, we could rescale the problem manually and would not need affine-invariant samplers. While the effect of the initial distribution may diminish over time in localized CBS (see, e.g., subsection 7.2 and Figure 3 in particular), choosing $D = \mathcal{C}(\rho_0)$ in localized ALDI ensures that an incorrectly scaled initial distribution persists.
- (ii) As in polarized CBS, localized ALDI uses weighted covariance matrices, which can be more expensive to compute than unweighted ones in localized CBS.

6 Discretizations and computational considerations

In this section, we bridge the gap between the theoretical localized CBS dynamics (29) and practical algorithms to solve problems of the form (1).

Particle discretization The dynamics (29) of localized CBS are defined as a McKean–Vlasov SDE: the law of U_t factors into its evolution. Of course, this law is not available in practice and (29) does not yet constitute an algorithm. We now introduce particle approximations, i.e., schemes where J approximate instances of (29) are run in parallel. They use their own empirical distribution instead of their unknown exact law to drive their evolution. We denote the i th particle by U_t^i and the entire ensemble by the $d \times J$ matrix $\mathbf{U}_t = (U_t^1, U_t^2, \dots, U_t^J)$.

When $\mathbf{C}(\rho_t; U_t)$ is an unweighted or weighted covariance, we replace it by a particle approximation: a (weighted) sample covariance of all particles defined as

$$\hat{\mathcal{C}}(\mathbf{U}) := \frac{1}{J} \sum_{j=1}^J (U^j - \hat{\mu}(\mathbf{U})) \otimes (U^j - \hat{\mu}(\mathbf{U})) \quad \text{with} \quad \hat{\mu}(\mathbf{U}) := \frac{1}{J} \sum_{j=1}^J U^j \quad (62)$$

for the unweighted covariance and, for the weighted covariance,

$$\hat{\mathcal{C}}_{\alpha, \lambda \hat{\mathcal{C}}(\mathbf{U})}(\mathbf{U}; U^i) := \sum_{j=1}^J \omega_{\alpha, \lambda \hat{\mathcal{C}}(\mathbf{U})}^{ij} (U^j - \hat{\mu}_{\alpha, \lambda \hat{\mathcal{C}}(\mathbf{U})}(\mathbf{U}; U^i)) \otimes (U^j - \hat{\mu}_{\alpha, \lambda \hat{\mathcal{C}}(\mathbf{U})}(\mathbf{U}; U^i)) \quad (63)$$

with

$$\hat{\mu}_{\alpha,A}(\mathbf{U}; U^i) := \sum_{j=1}^J \omega_{\alpha,A}^{ij} U^j, \quad (64)$$

where $\omega_{\alpha,A}^{ij} = w_{\alpha,A}^{ij} / \sum_{k=1}^J w_{\alpha,A}^{ik}$ with $w_{\alpha,A}^{ij} = w_{\alpha,A}(U_j; U_i)$. In general, we denote the particle approximation to $\mathbf{C}(\rho; U^i)$ by $\hat{\mathbf{C}}(\mathbf{U}; U^i)$. As in the mean-field setting of section 4, we assume that this preconditioner is invertible. Notably, this requires that the J particles span the entire space \mathbb{R}^d . While particle-based methods such as ALDI have been used with $J < d$ to sample in a linear subspace [20], we leave the application of localized CBS to those settings to future work.

We also replace the weighted mean in (29) by a particle approximation. The most straightforward option is a weighted sample mean of all particles, given in (64). Later in this section, we will also explore a random-batch modification of this scheme.

Time discretization After particle discretization, we are left with a system of interacting SDEs. Since studying time discretizations is not a main point of focus of this paper, we will use the standard Euler–Maruyama discretization with N timesteps of length Δt in our numerical tests, although others are possible⁶. We denote the i th particle at timestep n by U_n^i and the ensemble by \mathbf{U}_n .

Random-batch interaction For the weighted mean in the drift term of localized CBS, we introduce a different particle approximation that forbids self-to-self interaction (which would otherwise have very large weights when particles are sparsely distributed) and randomly subsamples particles with a factor $\nu \in (0, 1]$:

$$\hat{\mu}_{\beta, \kappa \hat{\mathbf{C}} / \beta}^{(\nu, i)}(\mathbf{U}_n; U_n^i) := \frac{\sum_{j=1}^J \mathbb{1}_{i \neq j \wedge \theta_n^{i,j} \leq \nu} U_n^j w_{\alpha, \lambda \hat{\mathbf{C}}}^{ij}}{\sum_{j=1}^J \mathbb{1}_{i \neq j \wedge \theta_n^{i,j} \leq \nu} w_{\alpha, \lambda \hat{\mathbf{C}}}^{ij}}. \quad (65)$$

Here, $\theta_n^{i,j}$ is uniformly random in $[0, 1]$ and we write $\hat{\mathbf{C}} := \hat{\mathbf{C}}(\mathbf{U}_n; U_n^i)$ for notational convenience. This idea is related to the random-batch method of [29], where interacting-particle systems are divided into small, random batches for a reduction in computational cost. When we use random batching, we will choose relatively large values of ν (e.g., $\nu = 0.5$), so the cost difference is moderate; instead, we are motivated by our observation that random-batch interaction can improve sampling performance for higher-dimensional, multimodal problems. This is illustrated in section 7.

Square-root-free formulation Similarly to what is proposed in [20], it is possible to replace the symmetric positive definite square root $\sqrt{\hat{\mathbf{C}}} \in \mathbb{R}^{d \times d}$ by a (rectangular) Cholesky factor $\hat{\mathbf{C}}^{1/2} \in \mathbb{R}^{d \times n}$, for any n , with the property that

$$\hat{\mathbf{C}} = \hat{\mathbf{C}}^{1/2} (\hat{\mathbf{C}}^{1/2})^T. \quad (66)$$

By using $\hat{\mathbf{C}}^{1/2}$ and simultaneously replacing the d -dimensional Brownian motion W_t by an n -dimensional one, the Fokker–Planck equation remains the same. Henceforth, we define $\bar{U} := \hat{\mu}(\mathbf{U})$, $\bar{U}^{(i)} := \hat{\mu}_{\alpha, \lambda \hat{\mathbf{C}}(\mathbf{U})}(\mathbf{U}; U^i)$, $w^{ij} := w_{\alpha, \lambda \hat{\mathbf{C}}(\mathbf{U})}^{ij}$, and $\omega^{ij} := \omega_{\alpha, \lambda \hat{\mathbf{C}}(\mathbf{U})}^{ij}$ for conciseness. The unweighted and weighted covariance have factors

$$\hat{\mathbf{C}}^{1/2}(\mathbf{U}) = \frac{1}{\sqrt{J}} \begin{bmatrix} (U^1 - \bar{U}) & \dots & (U^J - \bar{U}) \end{bmatrix} \quad (67)$$

⁶Classical CBS uses a non-standard timestepping scheme, which helps them prove properties in the time-discrete setting. Polarized CBS adopts this same method. While EKS uses a linearly implicit split-step time discretization, both ALDI and localized ALDI use standard Euler–Maruyama.

and

$$\hat{\mathcal{C}}_{\alpha, \lambda \hat{\mathcal{C}}(\mathbf{U})}^{1/2}(\mathbf{U}; U^i) = \left[\sqrt{\omega^{i1}} (U^1 - \bar{U}^{(i)}) \quad \dots \quad \sqrt{\omega^{iJ}} (U^J - \bar{U}^{(i)}) \right], \quad (68)$$

respectively. These are readily available and avoid computing the square root of $\hat{\mathbf{C}}$. This should offer computational advantages unless $J \gg d$.

Covariance-weighted norms In the weight function (24), localized CBS uses preconditioner-weighted squared norms $\|U^i - U^j\|_{\hat{\mathbf{C}}}^2 = (U^i - U^j)^T \hat{\mathbf{C}}^{-1} (U^i - U^j)$. This quantity can be evaluated as follows: precompute

$$M := \mathbf{U}^T \hat{\mathbf{C}}^{-1} \mathbf{U}$$

and use

$$\|U^i - U^j\|_{\hat{\mathbf{C}}}^2 = M_{ii} + M_{jj} - 2M_{ij}.$$

If $\hat{\mathbf{C}}$ depends on i , then so does M .

Correction term The discretized dynamics contain the correction term $\nabla_{u^i} \cdot \hat{\mathbf{C}}$, where $\hat{\mathbf{C}} := \hat{\mathbf{C}}(\mathbf{U}_n; U_n^i)$. We now study this term for the preconditioners we consider in this article. When $\hat{\mathbf{C}} = K$, clearly $\nabla_{u^i} \cdot \hat{\mathbf{C}} = 0$. When $\hat{\mathbf{C}} = \hat{\mathcal{C}}_{\alpha, \lambda \hat{\mathcal{C}}(\mathbf{U})}(\mathbf{U}; U)$, the correction term is given in Lemma 7. The preconditioners $\hat{\mathcal{C}}_{\alpha}(\mathbf{U})$ and $\hat{\mathcal{C}}(\mathbf{U})$ correspond to Lemma 7 with $\lambda = \infty$ and, in the latter case, $\alpha = 0$ as well. Note that the correction term contains a derivative of $\hat{\pi}$ when $\alpha \neq 0$, which is problematic in our otherwise derivative-free method. In this paper we always choose $\alpha = 0$. If situations are identified where $\alpha \neq 0$ is preferred, one could neglect the $\hat{\pi}$ derivatives (see Remark 8) or construct a particle approximation (e.g., based on the proximal operator such as in section 3 or on the technique in [53]). This is left for future work.

Lemma 7. *When $\hat{\mathbf{C}} = \hat{\mathcal{C}}_{\alpha, \lambda \hat{\mathcal{C}}(\mathbf{U})}(\mathbf{U}; U^i)$, it holds that*

$$\begin{aligned} \nabla_{u^i} \cdot \hat{\mathbf{C}} &= \omega^{ii} (d+1) U_c^{(i),i} + \frac{1}{\lambda} U_c^{(i)} \left(\omega^i \odot \text{diag}((U_c^{(i)})^T \hat{\mathcal{C}}^{-1} U_c^{(i)}) \right) \\ &\quad - \frac{1}{\lambda J} \hat{\mathbf{C}} \hat{\mathcal{C}}^{-1} \left(U_c^{(i),i} (U_c^{(i),i})^T + \hat{\mathbf{C}} \right) \hat{\mathcal{C}}^{-1} U_c^i \\ &\quad + \frac{1}{\lambda J} U_c^{(i)} \left(\omega^i \odot \text{diag}((U_c^{(i)})^T \hat{\mathcal{C}}^{-1} (\mathbf{U} - U^i \mathbf{1}^T)) \odot ((U_c^i)^T \hat{\mathcal{C}}^{-1} (\mathbf{U} - U^i \mathbf{1}^T))^T \right) \\ &\quad + \alpha \omega^{ii} \left(U_c^{(i),i} (U_c^{(i),i})^T - \hat{\mathbf{C}} \right) \frac{\nabla_{u^i} \hat{\pi}(U^i)}{\hat{\pi}(U^i)}, \end{aligned} \quad (69)$$

where \odot denotes the Hadamard (elementwise) product, $\mathbf{U}_c := \mathbf{U} - \bar{\mathbf{U}} \mathbf{1}^T$, $\mathbf{U}_c^{(i)} := (\mathbf{U} - \bar{\mathbf{U}}^{(i)} \mathbf{1}^T)$, U_c^i is the i th column of \mathbf{U}_c , $U_c^{(i),j}$ is the j th column of $\mathbf{U}_c^{(i)}$, $\hat{\mathbf{C}}$ is a shorthand for $\hat{\mathcal{C}}(\mathbf{U})$, and $\omega^i = (\omega^{i1}, \dots, \omega^{iJ})^T$.

Proof. This is proven in Appendix A. □

Remark 8. *All terms in (69) except the second go down in magnitude as the number of particles J increases (through either $1/J$ or $\omega^{ii} = w^{ii} / \sum_j w^{ij}$, which depends on J due to the normalization). It may be computationally interesting to omit some of these terms in practice when J is large.*

Localized CBS algorithm Combining the points discussed in this section leads to the localized CBS algorithm

$$U_{n+1}^i = U_n^i + \left[-\frac{\gamma}{\kappa} \left(U_n^i - \hat{\mu}_{\beta, \kappa \hat{\mathbf{C}}/\beta}^{(\nu, i)}(\mathbf{U}_n; U_n^i) \right) + \nabla_{u^i} \cdot \hat{\mathbf{C}} \right] \Delta t + \sqrt{2\Delta t} \hat{\mathbf{C}}^{1/2} \xi_n^i, \quad (70)$$

with $\xi_n^i \sim \mathcal{N}(0, I)$ i.i.d. random variables.

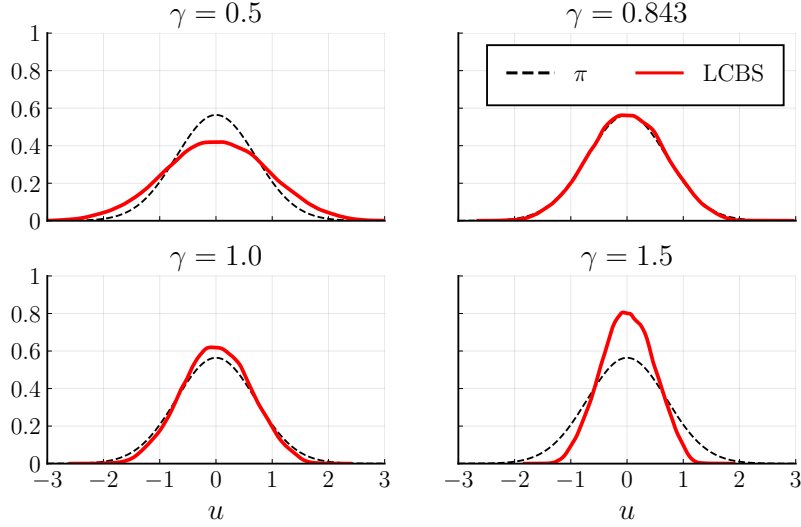


Figure 1: Localized CBS samples for a one-dimensional Gaussian target distribution

7 Numerical results

In this section, we apply the localized CBS algorithm to a variety of problems, illustrating its properties. For both localized CBS and alternative methods, we will use Euler–Maruyama time discretizations. Unless mentioned otherwise, localized CBS uses timestep $\Delta t = 0.01$ and preconditioner $\mathcal{C}(\rho_t)$, an unweighted covariance. The default random-batch parameter is $\nu = 1$, such that a particle interacts with all other particles. In addition, except in subsection 7.3, we obtain samples of all considered methods by running the algorithm with the specified parameters 16 times, and combining the particle positions at all time steps within the final quarter of the time interval in each run. Samples are plotted with the `density` function from the Julia package `StatsPlots`, which performs kernel density estimation (KDE) to smooth the samples into an approximate distribution. When the dimension d is larger than one, the plots show the marginal distribution in the first dimension unless specified otherwise. The initial distribution for all sampling methods will be a zero-centered Gaussian $\mathcal{N}(0, \Sigma_0)$; by default, $\Sigma_0 = I/2$. Our code is located at

<https://gitlab.kuleuven.be/numa/public/paper-code-lcbs>.

7.1 Gaussian distributions

We apply localized CBS to a Gaussian distribution, to verify the values of γ we obtained in subsection 4.3 and to assess the influence of γ on the sampled distribution. We consider the one-dimensional potential function

$$V(u) = u^2 \quad (71)$$

and use $(\beta, \kappa) = (5.0, 0.01)$, $J = 500$ particles, and $N = 200$ timesteps. Figure 1 shows the resulting samples with $\gamma \in \{0.5, \bar{\gamma}, 1.0, 1.5\}$, where $\bar{\gamma} \approx 0.843$ is the value given by (38)—since we use our default preconditioner $\mathcal{C}(\rho_t)$, this should ensure correct sampling for Gaussians. When $\gamma < \bar{\gamma}$, there is insufficient drift towards the weighted mean and the samples are too spread out. When $\gamma > \bar{\gamma}$, the opposite effect occurs. As predicted by the theory, the distribution is sampled correctly with $\gamma = \bar{\gamma}$.

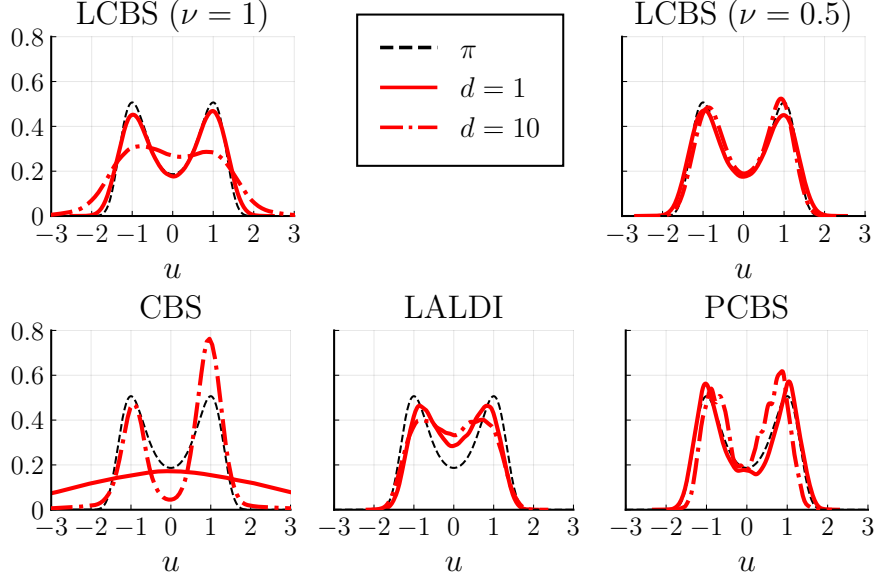


Figure 2: Marginalized samples for a 1- or 10-dimensional multimodal target distribution. Recall that we aggregate the samples from 16 runs, which explains the non-Gaussian CBS samples.

7.2 Multimodal distributions

One of the design objectives of localized CBS is to handle non-Gaussian, potentially even multimodal, distributions. The first multimodal distribution that we consider corresponds to the potential function

$$V(u) = \|u^2 - 1\|^2, \quad (72)$$

where u^2 applies the exponent elementwise. The resulting distribution π is bimodal when the dimension d is 1 and a tensor product of bimodal distributions otherwise.

For this potential and with $d \in \{1, 10\}$, we compare localized CBS (with $\beta = 10$ and $\kappa = 0.03$) to CBS (with $\alpha = 10$ and $\Delta t = 0.01$), polarized CBS (with $\alpha = 10$, $\lambda = 0.005$ when $d = 1$ or $\lambda = 0.1$ when $d = 10$, $D = I$, and $\Delta t = 0.01$), and localized ALDI (with $\lambda = 0.02$ when $d = 1$ or $\lambda = 0.4$ when $d = 10$, $D = I$, and $\Delta t = 0.02$). All tests use $J = 200$ particles and $N = 1000$ timesteps. For localized CBS, we additionally compare $\nu = 1$ to $\nu = 0.5$. Figure 2 shows the resulting samples. Localized CBS accurately finds the distribution when $d = 1$; when $d = 10$, we get a good approximation only with random-batch interaction turned on ($\nu = 0.5$). Localized ALDI and polarized CBS each give relatively close approximations, but are unable to exactly fit π . Note also that for these two methods, unlike for localized CBS, we needed to hand-tune the parameters for each d . Classical CBS finds the multiple modes only when $d = 10$, and fails to approximate the density in between.⁷

Secondly, we study affine-invariance of the three best performing algorithms: localized CBS, polarized CBS, and localized ALDI. To this end, consider

$$V(u) = \|(\sqrt{\Lambda}u)^2 - 1\|^2, \quad (73)$$

where u is $(d = 2)$ -dimensional and the square again applies elementwise. The matrix $\Lambda = \text{diag}(1, 10^4)$ changes the scale of the second parameter. Suppose that we may not know this scaling before solving the problem. Without knowing the form of the potential (73), we

⁷Note that the particles in CBS always follow a Gaussian distribution; in our experiment, CBS captures multiple modes as the results from 16 runs (which may find different modes) are aggregated.

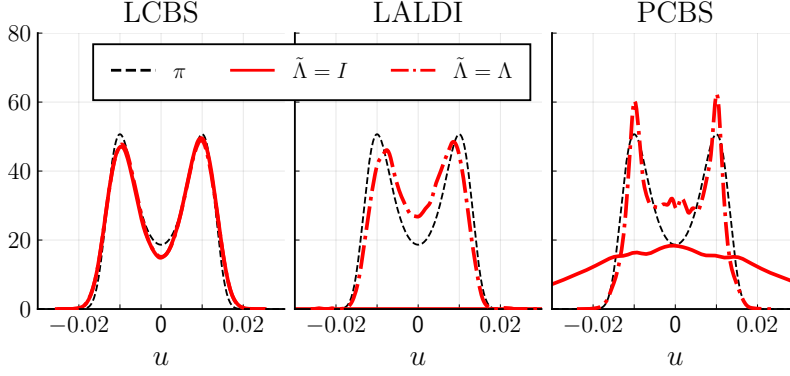


Figure 3: Marginalized samples for a 2-dimensional poorly scaled multimodal target distribution. In the left figure, the two red lines are visually indistinguishable; in the middle figure, the line for $\tilde{\Lambda} = I$ coincides with the horizontal axis as the samples diverge.

assume that the relative scaling of the two parameters is given by a scaling matrix $\tilde{\Lambda}$ that can either be the correct $\tilde{\Lambda} = \Lambda$ or the incorrect $\tilde{\Lambda} = I$. We use this assumption to choose an initial covariance $\Sigma_0 = \tilde{\Lambda}^{-1}/2$. Furthermore,

- (i) in polarized CBS and localized ALDI, we set $D = \tilde{\Lambda}^{-1}$;
- (ii) in our localized CBS algorithm, we simply use the preconditioner $\mathcal{C}(\rho_t)$, which does not need *a priori* scaling information.

We use $(\beta, \kappa) = (10, 0.03)$ for localized CBS, $\lambda = 0.02$ and $\Delta t = 0.05$ for localized ALDI, and $\lambda = 0.005$ for polarized CBS. Figure 3 shows the values sampled by these algorithms for both $\tilde{\Lambda}$ cases. Polarized CBS and localized ALDI perform as expected when the scaling is guessed correctly, but generate clearly incorrect samples when it is not. This is because they depend on $\tilde{\Lambda}$ not only for their initial condition, but also for weighting the distance between particles throughout the algorithm. Localized CBS, on the other hand, proves itself able to recover from this poor initial guess and produces good—and almost identical—samples for both $\tilde{\Lambda}$ s.

Now consider a different potential function with $d = 1$:

$$V(u) = 2(u \exp(u))^4 - 4(u \exp(u))^2 - 2(u/3)^5 + 2. \quad (74)$$

This again yields a multimodal distribution, now with one wide and one narrow peak. We first use (74) to compare different preconditioners for localized CBS. We choose parameters $(\beta, \kappa) = (10, 0.02)$ with $N = 1000$ timesteps and $J = 200$ particles. As preconditioner, we use the weighted covariance $\mathcal{C}_{0, \lambda \mathcal{C}(\rho_t)}(\rho_t; U_t)$ with $\lambda \in \{0.1, 0.5, \infty\}$. Note that, when $\lambda = \infty$, this corresponds to the unweighted covariance $\mathcal{C}(\rho_t)$. The initial distribution has covariance $\Sigma_0 \in \{I/2, 2I\}$. Resulting samples are shown in Figure 4. When $\lambda = \infty$, the global nature of the preconditioner means that the presence of the wide peak causes the narrow one to be estimated poorly. The value $\lambda = 0.1$, on the other hand, is too small and localized CBS struggles to find the full distribution when the initial distribution is too narrow. A moderate value of $\lambda = 0.5$ seems to combine the benefits of both extremes. Note that, as discussed in subsection 4.2, $\lambda = \infty$ has the computational advantage that only one covariance needs to be computed instead of J different ones.

Next, we illustrate the importance of the correction term $\nabla_u \cdot \mathbf{C}_{U,t}$ in the localized CBS dynamics (29) on the sampling problem (74). We consider the preconditioner $\mathcal{C}_{0, \lambda \mathcal{C}(\rho_t)}(\rho_t; U_t)$ with $\lambda = 0.5$ and compare the normal localized CBS algorithm to a modified version where the correction term is omitted. We also apply polarized CBS, which does not have a similar

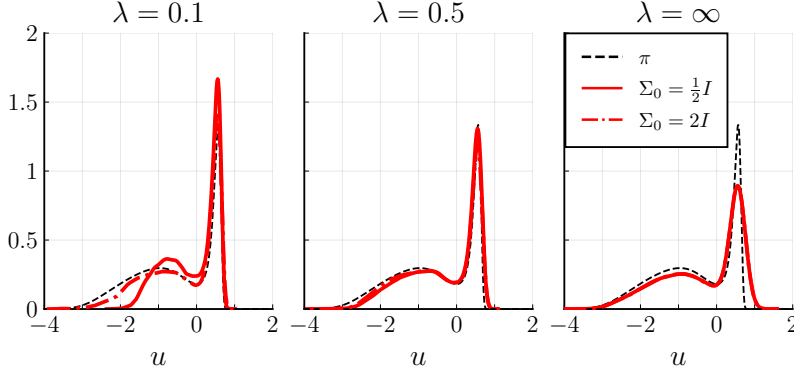


Figure 4: Localized CBS samples for (74) with various preconditioners and initial distributions

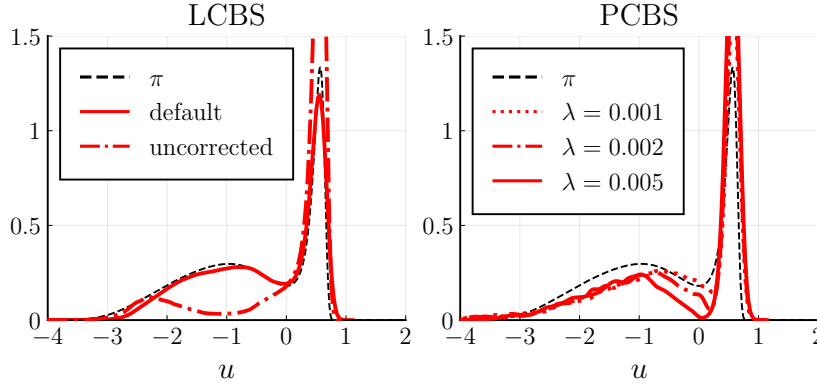


Figure 5: Localized and polarized CBS samples for (74)

correction term, with $\alpha = 10$ and $\lambda \in \{0.001, 0.002, 0.005\}$. We use $N = 1000$ timesteps, $J = 200$ particles, and an initial covariance $\Sigma_0 = 2I$ for all samplers. Figure 5 illustrates that only localized CBS with the correction term manages to accurately retrieve π . As before, polarized CBS only samples from a distribution approximating π .

7.3 A tent-shaped distribution

In the next example we study convergence of localized CBS for the one-dimensional target distribution corresponding to

$$\pi(u) = \hat{\pi}(u) = \max(0, 1 - |u|), \quad (75)$$

a tent-shaped distribution with finite support. We will answer the question why, even though $\beta \rightarrow \infty$ and $\kappa \rightarrow 0$ seem desirable, it may still make sense to choose moderate values for both parameters. In Figure 6, we show the Wasserstein-2 distance between the exact distribution π and the empirical distribution of localized CBS ensembles with a given number J of particles. This is compared for several (β, κ) combinations. In this subsection, we find the empirical distribution for any (β, κ, J) by simulating localized CBS 480 times and, for each simulation, using the positions of 50 randomly chosen particles at the final time step as samples.

After a certain value, increasing J no longer improves accuracy. This is caused by the discrepancy between the mean-field distribution and π , which decreases with large β and small κ . However, these more accurate mean-field dynamics become increasingly difficult to approximate with a finite number of particles, as fewer particles get to contribute substantially

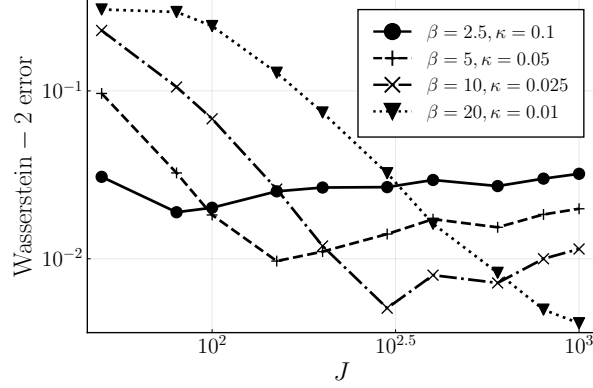


Figure 6: Wasserstein-2 error between the localized CBS samples and the target distribution (75)

to the weighted means. Hence, when large numbers of particles are computationally feasible, a high accuracy can be obtained by choosing $\beta \gg 0$ and $\kappa \approx 0$. When relatively few particles can be used, on the other hand, the accuracy is actually highest for more moderate β and κ choices.

Remark 9. When J keeps increasing, the errors in Figure 6 become slightly larger again. This could be caused by a combination of two factors: (i) the Moreau envelope step in section 3 approximates π by a distribution with longer tails and (ii) when J is small, localized CBS tends to undersample the tails. While the first factor is a source of error that is present for all J , the second factor may partially offset it for small J , resulting in an error smaller than that for $J \rightarrow \infty$.

7.4 A Darcy flow inverse problem

Consider a two-dimensional spatial domain $\Omega := [0, 1]^2$. The Darcy flow inverse problem is to recover parameters u of the permeability field $a(x, u)$ from noisy measurements of the pressure field $p(x)$ satisfying

$$-\nabla \cdot (a(x, u) \nabla p(x)) = f(x), \quad x \in \Omega, \quad (76a)$$

$$p(x) = 0, \quad x \in \partial\Omega. \quad (76b)$$

Here, $f(x) = c$ is a fluid source that we set to a constant value.

The permeability $a(x, u)$ is modeled as a log-normal random field with mean zero and covariance operator $(-\Delta + \tau^2)^{-s}$ of $\log a$, where $-\Delta$ represents the Laplacian with homogeneous Neumann boundary conditions. This corresponds to a standard normal prior on the parameters u_k in the Karhunen–Loève (KL) expansion

$$\log a(x, u) = \sum_{k \in \mathbb{N}^2 \setminus \{(0,0)\}} u_k \sqrt{\lambda_k} \phi_k(x), \quad (77)$$

with eigenpairs given by $\lambda_k = (\pi^2 \|k\|^2 + \tau^2)^{-s}$ and $\phi_k = c_k \cos(\pi k_1 x_1) \cos(\pi k_2 x_2)$, where $c_k = \sqrt{2}$ if $k_1 k_2 = 0$ and $c_k = 1$ otherwise (see, e.g., [27]). We choose parameters $(\tau, s) = (3, 2)$ and truncate the expansion (77) after the d terms with largest eigenvalues λ_k . The coefficients u_k of these terms are the unknown parameters u with prior $\pi_{\text{prior}} = \mathcal{N}(0, \Gamma_0)$, with $\Gamma_0 = I$, in the Bayesian inverse problem (2). The data y consists of measurements of p , taken at 49 equispaced points and subject to noise known to be distributed according to $\pi_{\text{noise}} = \mathcal{N}(0, \Gamma)$

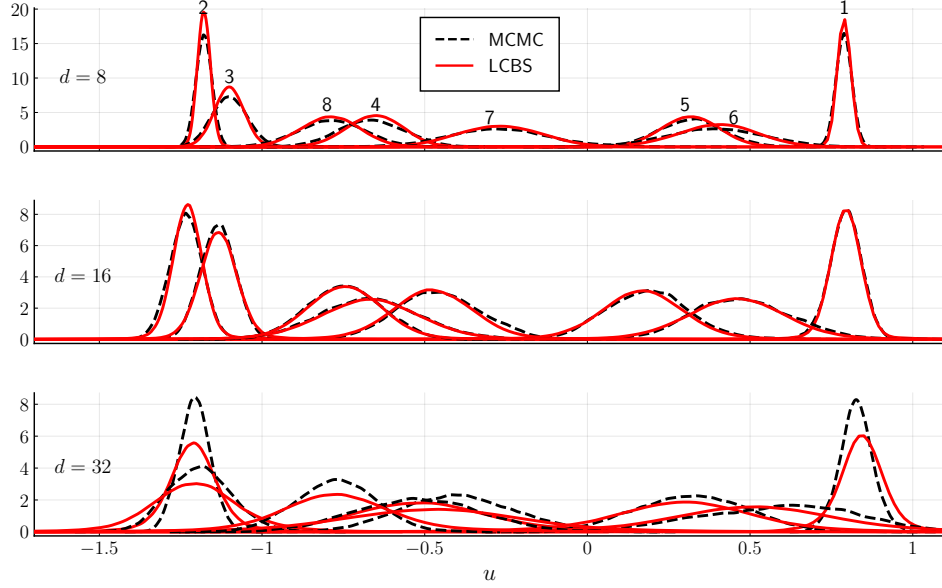


Figure 7: Random-walk Markov chain Monte Carlo and localized CBS approximations to the distributions of the first 8 KL terms in the d -dimensional Darcy flow problem, with $d \in \{8, 16, 32\}$. The $d = 8$ plot labels the modes in order of decreasing eigenvalue λ_k .

with $\Gamma = 10^{-4}I$. The model G solves (76) with central finite differences on a grid with step-size $h = 2^{-5}$. An observation is generated by sampling $\{u_k\}_k$ from the prior, solving (76) with stepsize $h = 2^{-9}$, and perturbing that solution with a random sample from π_{noise} . As described in subsection 1.1, this Bayesian inverse problem corresponds to (1) with

$$V(u) = \frac{1}{2}\|y - G(u)\|_{\Gamma}^2 + \frac{1}{2}\|u\|_{\Gamma_0}^2. \quad (78)$$

We solve this inverse problem with random-walk MCMC (as a reference solution) and localized CBS. We use $N = 400$ timesteps of length $\Delta t = 0.03$, $J = 1000$ particles, and a large initial covariance $\Sigma_0 = 9I$ (similarly to [6]). Since Γ is small, we expect the posterior to be close to Gaussian, which is also confirmed by the MCMC reference solution. Hence, we choose moderate parameters $(\beta, \kappa) = (3, 0.2)$. Figure 7 compares the MCMC samples to the localized CBS samples. It shows the marginalized distributions for the first 8 modes, for the number of dimensions $d \in \{8, 16, 32\}$. The modes are successfully located for all d values. For each d , the MCMC modes are recovered accurately by localized CBS. When $d = 8$ or $d = 16$, the uncertainty around the mode is captured well; when $d = 32$, it is slightly overestimated.

8 Conclusions

We proposed a novel interacting-particle method for sampling from non-Gaussian distributions, based on an alternative interpretation of consensus-based sampling (CBS) as an approximation to interacting Langevin diffusions. In the mean-field limit, our *localized CBS* method was shown to have desirable properties such as affine-invariance and unbiased sampling from Gaussian distributions.

Numerical experiments showed that localized CBS deals well with poorly scaled sampling problems, even when this scaling is unknown in advance. It is also able to accurately identify multiple modes in problems with low or moderate dimension.

Localized CBS has several parameters, including a preconditioner that can be chosen very broadly. In our experiments, we have focused on the simple preconditioner $\mathcal{C}(\rho_t)$ —an unweighted covariance of the SDE’s law at time t —and briefly explored a more complex space-dependent preconditioner. Future research could focus on studying the choice of the preconditioner and other parameters in more detail. In addition, it would be very valuable to obtain convergence results for localized CBS with a finite number of particles. These results could also elucidate the precise role played by random-batch interaction, which appears critical to the performance of localized CBS in some multimodal higher-dimensional problems.

More broadly, a detailed study of the influence of timestepping schemes on the efficiency and accuracy of samplers based on interacting particles is likely to make these methods more practical as a whole. In this context, the adaptive timestepping scheme developed in [32] for ensemble Kalman inversion—and used in [19] for ensemble Kalman sampling—is a promising example.

Acknowledgments

We are grateful to Kathrin Hellmuth for her comments on an earlier draft of this paper. Our work was partially funded by the Research Foundation – Flanders (FWO) (grants 1169725N, G081222N, G033822N, and G0A0920N) and the KU Leuven Research Council (C1 projects C14/23/098 and C14/24/103).

A Various technical proofs

In this appendix, we give proofs for some results used in the main text.

Proof of (26), (34), and (35). Consider means (m, m_t) and covariances (Σ, Σ_t) such that $\pi \sim \mathcal{N}(m, \Sigma)$ and $\rho_t \sim \mathcal{N}(m_t, \Sigma_t)$. We prove (26) by computing

$$\mu_\alpha(\rho_t) = \frac{\int v \exp(-\frac{\alpha}{2}\|v - m\|_\Sigma^2) \exp(-\frac{1}{2}\|v - m_t\|_{\Sigma_t}^2) dv}{\int \exp(-\frac{\alpha}{2}\|v - m\|_\Sigma^2) \exp(-\frac{1}{2}\|v - m_t\|_{\Sigma_t}^2) dv}, \quad (79)$$

which is the mean of the product of two Gaussians, $\mathcal{N}(m, \Sigma/\alpha)$ and $\mathcal{N}(m_t, \Sigma_t)$. We use the formula found in, e.g., [45, §8.1.8] to compute $\mu_\alpha(\rho_t)$ and, similarly, $\mathcal{C}_\alpha(\rho_t)$:

$$\mu_\alpha(\rho_t) = (\alpha\Sigma^{-1} + \Sigma_t^{-1})^{-1}(\alpha\Sigma^{-1}m + \Sigma_t^{-1}m_t) \quad \text{and} \quad \mathcal{C}_\alpha(\rho_t) = (\alpha\Sigma^{-1} + \Sigma_t^{-1})^{-1}. \quad (80)$$

Then, $\mu_{\beta, \kappa \mathcal{C}_\alpha(\rho_t)/\beta}(\rho_t; U_t)$ is given by

$$\begin{aligned} & \frac{\int v \exp(-\frac{\beta}{2\kappa}\|v - U_t\|_{\mathcal{C}_\alpha(\rho_t)}^2) \exp(-\frac{\beta}{2}\|v - m\|_\Sigma^2) \exp(-\frac{1}{2}\|v - m_t\|_{\Sigma_t}^2) dv}{\int \exp(-\frac{\beta}{2\kappa}\|v - U_t\|_{\mathcal{C}_\alpha(\rho_t)}^2) \exp(-\frac{\beta}{2}\|v - m\|_\Sigma^2) \exp(-\frac{1}{2}\|v - m_t\|_{\Sigma_t}^2) dv} \\ &= \left(\frac{\beta}{\kappa}(\alpha\Sigma^{-1} + \Sigma_t^{-1}) + \beta\Sigma^{-1} + \Sigma_t^{-1} \right)^{-1} \left(\frac{\beta}{\kappa}(\alpha\Sigma^{-1} + \Sigma_t^{-1})U_t + \beta\Sigma^{-1}m + \Sigma_t^{-1}m_t \right) \\ &= \left(\beta \left(\frac{\alpha}{\kappa} + 1 \right) \Sigma^{-1} + \left(\frac{\beta}{\kappa} + 1 \right) \Sigma_t^{-1} \right)^{-1} \left(\frac{\beta}{\kappa}(\alpha\Sigma^{-1} + \Sigma_t^{-1})U_t + \beta\Sigma^{-1}m + \Sigma_t^{-1}m_t \right). \end{aligned}$$

Filling in $\kappa = \beta = \alpha$, we compute

$$\begin{aligned} & (\alpha + 1) \frac{\gamma}{\kappa} (U_t - \mu_{\beta, \kappa \mathcal{C}_\alpha(\rho_t)/\beta}(\rho_t; U_t)) \\ &= 2 \left[U_t - (2\alpha\Sigma^{-1} + 2\Sigma_t^{-1})^{-1} ((\alpha\Sigma^{-1} + \Sigma_t^{-1})U_t + \alpha\Sigma^{-1}m + \Sigma_t^{-1}m_t) \right] \\ &= U_t - (\alpha\Sigma^{-1} + \Sigma_t^{-1})^{-1} (\alpha\Sigma^{-1}m + \Sigma_t^{-1}m_t) = U_t - \mu_\alpha(\rho_t). \end{aligned}$$

Equations (34a) and (34b) follow directly from the definitions. Equations (34c), (34d), and (35) are derived similarly to $\mu_{\beta, \kappa \mathcal{C}_\alpha(\rho_t)/\beta}(\rho_t; U_t)$ above. \square

Proof of Lemma 7. In [47, Lemma 3.11], the divergence of a weighted covariance with general weight function is given:

$$\nabla_{u^i} \cdot \hat{\mathbf{C}} = \omega^{ii} (d+1)(U^i - \bar{U}^{(i)}) + \sum_{j=1}^J \left(U_c^{(i),j} (U_c^{(i),j})^T - \bar{U}^{(i)} (\bar{U}^{(i)})^T \right) \nabla_{u^i} \omega^{ij}. \quad (81)$$

With our weight function, we find that

$$\begin{aligned} \nabla_{u^i} \omega^{ij} &= \nabla_{u^i} \left(\omega^{ij} / \sum_{k=1}^J \omega^{ik} \right) = \left(\nabla_{u^i} \omega^{ij} - \omega^{ij} \nabla_{u^i} \left(\sum_{k=1}^J \omega^{ik} \right) \right) / \sum_{k=1}^J \omega^{ik} \\ &= \left[-\frac{1}{2\lambda} \left(2\hat{\mathcal{C}}^{-1}(U^i - U^j) - X^{ij} \right) + \delta^{ij} \alpha \frac{\nabla_{u^i} \hat{\pi}(U^i)}{\hat{\pi}(U^i)} \right] \omega^{ij} \\ &\quad + \omega^{ij} \sum_{k=1}^J \left[\frac{1}{2\lambda} \left(2\hat{\mathcal{C}}^{-1}(U^i - U^k) - X^{ik} \right) - \delta^{ik} \alpha \frac{\nabla_{u^i} \hat{\pi}(U^i)}{\hat{\pi}(U^i)} \right] \omega^{ik} \\ &= \frac{\omega^{ij}}{\lambda} \left([\hat{\mathcal{C}}^{-1}(U^j - U^i) + \frac{X^{ij}}{2}] + [\hat{\mathcal{C}}^{-1}U_c^{(i),i} - \sum_{k=1}^J \omega^{ik} \frac{X^{ik}}{2}] \right) \\ &\quad + (\delta^{ij} - \omega^{ij}) \alpha \omega^{ii} \frac{\nabla_{u^i} \hat{\pi}(U^i)}{\hat{\pi}(U^i)} \\ &= \frac{\omega^{ij}}{\lambda} \left(\hat{\mathcal{C}}^{-1}U_c^{(i),j} - \sum_{k=1}^J \omega^{ik} \frac{X^{ik}}{2} + \frac{X^{ij}}{2} \right) + (\delta^{ij} - \omega^{ij}) \alpha \omega^{ii} \frac{\nabla_{u^i} \hat{\pi}(U^i)}{\hat{\pi}(U^i)}, \end{aligned}$$

where X^{ik} is a vector whose ℓ th element is $(U^i - U^k)^T \hat{\mathcal{C}}^{-1} (\partial_{u_\ell^i} \hat{\mathcal{C}}) \hat{\mathcal{C}}^{-1} (U^i - U^k)$, with $\partial_{u_\ell^i} \hat{\mathcal{C}} = J^{-1} (U_c^i e_\ell^T + e_\ell (U_c^i)^T)$. It can be verified that

$$X^{ij}/2 = J^{-1} ((U_c^i)^T \hat{\mathcal{C}}^{-1} (U^i - U^j)) \hat{\mathcal{C}}^{-1} (U^i - U^j), \quad (82a)$$

$$\sum_{k=1}^J X^{ik} \omega^{ik}/2 = J^{-1} \hat{\mathcal{C}}^{-1} (U_c^{(i),i} (U_c^{(i),i})^T + \hat{\mathbf{C}}) \hat{\mathcal{C}}^{-1} U_c^i. \quad (82b)$$

We split $\nabla_{u^i} \cdot \hat{\mathbf{C}} = A + (B_1 + B_2 + B_3 - C_1 - C_2 - C_3)/\lambda + D$ with

$$\begin{aligned} A &:= \omega^{ii} (d+1)(U^i - \bar{U}^{(i)}), \\ B_1 &:= \sum_{j=1}^J U_c^{(i),j} (U_c^{(i),j})^T \omega^{ij} [\hat{\mathcal{C}}^{-1} U_c^{(i),j}] \\ &= U_c^{(i)} (\omega^i \odot \text{diag}((U_c^{(i)})^T \hat{\mathcal{C}}^{-1} U_c^{(i)})), \\ B_2 &:= \sum_{j=1}^J U_c^{(i),j} (U_c^{(i),j})^T \omega^{ij} [-J^{-1} \hat{\mathcal{C}}^{-1} (U_c^{(i),i} (U_c^{(i),i})^T + \hat{\mathbf{C}}) \hat{\mathcal{C}}^{-1} U_c^i] \\ &= -J^{-1} \hat{\mathbf{C}} \hat{\mathcal{C}}^{-1} (U_c^{(i),i} (U_c^{(i),i})^T + \hat{\mathbf{C}}) \hat{\mathcal{C}}^{-1} U_c^i, \\ B_3 &:= \sum_{j=1}^J U_c^{(i),j} (U_c^{(i),j})^T \omega^{ij} [J^{-1} ((U_c^i)^T \hat{\mathcal{C}}^{-1} (U^i - U^j)) \hat{\mathcal{C}}^{-1} (U^i - U^j)] \\ &= J^{-1} U_c^{(i)} (\omega^i \odot \text{diag}((U_c^{(i)})^T \hat{\mathcal{C}}^{-1} (U - U^i \mathbf{1}^T)) \odot ((U_c^i)^T \hat{\mathcal{C}}^{-1} (U - U^i \mathbf{1}^T))^T), \end{aligned}$$

$$\begin{aligned}
C_1 &:= \sum_{j=1}^J \bar{U}^{(i)} (\bar{U}^{(i)})^T \omega^{ij} [\hat{\mathcal{C}}^{-1} U_c^{(i),j}] = \bar{U}^{(i)} (\bar{U}^{(i)})^T \hat{\mathcal{C}}^{-1} \left(\sum_{j=1}^J \omega^{ij} U_c^{(i),j} \right) = 0, \\
C_2 &:= \sum_{j=1}^J \bar{U}^{(i)} (\bar{U}^{(i)})^T \omega^{ij} \left[- \sum_{k=1}^J \omega^{ik} \frac{X^{ik}}{2} \right] = -\bar{U}^{(i)} (\bar{U}^{(i)})^T \sum_{k=1}^J \omega^{ik} \frac{X^{ik}}{2}, \\
C_3 &:= \sum_{j=1}^J \bar{U}^{(i)} (\bar{U}^{(i)})^T \omega^{ij} \left[\frac{X^{ij}}{2} \right] = \bar{U}^{(i)} (\bar{U}^{(i)})^T \sum_{j=1}^J \omega^{ij} \frac{X^{ij}}{2} = -C_2, \\
D &:= \sum_{j=1}^J \left(U_c^{(i),j} (U_c^{(i),j})^T - \bar{U}^{(i)} (\bar{U}^{(i)})^T \right) (\delta^{ij} - \omega^{ij}) \alpha \omega^{ii} \frac{\nabla_{u^i} \hat{\pi}(U^i)}{\hat{\pi}(U^i)} \\
&= \alpha \omega^{ii} \left(U_c^{(i),i} (U_c^{(i),i})^T - \hat{\mathbf{C}} \right) \frac{\nabla_{u^i} \hat{\pi}(U^i)}{\hat{\pi}(U^i)}.
\end{aligned}$$

□

References

- [1] O. AL-GHATTAS AND D. SANZ-ALONSO, *Non-asymptotic analysis of ensemble Kalman updates: Effective dimension and localization*, Inf. Inference J. IMA, 13 (2024), p. iaad043.
- [2] J. BESAG, *Discussion of the Paper by Grenander and Miller*, J. R. Stat. Soc. B, 56 (1994), pp. 591–592.
- [3] S. BROOKS, A. GELMAN, G. JONES, AND X.-L. MENG, eds., *Handbook of Markov Chain Monte Carlo*, Chapman and Hall/CRC, New York, May 2011.
- [4] L. BUNGER, T. ROITH, AND P. WACKER, *Polarized consensus-based dynamics for optimization and sampling*, Math. Program., (2024).
- [5] J. A. CARRILLO, Y.-P. CHOI, C. TOTZECK, AND O. TSE, *An analytical framework for consensus-based global optimization method*, Math. Models Methods Appl. Sci., 28 (2018), pp. 1037–1066.
- [6] J. A. CARRILLO, F. HOFFMANN, A. M. STUART, AND U. VAES, *Consensus-based sampling*, Stud. Appl. Math., 148 (2022), pp. 1069–1140.
- [7] N. K. CHADA, Y. CHEN, AND D. SANZ-ALONSO, *Iterative ensemble Kalman methods: A unified perspective with some new variants*, Found. Data Sci., 3 (2021), pp. 331–369.
- [8] S. L. COTTER, G. O. ROBERTS, A. M. STUART, AND D. WHITE, *MCMC Methods for Functions: Modifying Old Algorithms to Make Them Faster*, Stat. Sci., 28 (2013), pp. 424–446.
- [9] T. CUI, K. J. H. LAW, AND Y. M. MARZOUK, *Dimension-independent likelihood-informed MCMC*, J. Comput. Phys., 304 (2016), pp. 109–137.
- [10] M. DASHTI, K. J. H. LAW, A. M. STUART, AND J. VOSS, *MAP estimators and their consistency in Bayesian nonparametric inverse problems*, Inverse Probl., 29 (2013), p. 095017.
- [11] P. DEL MORAL, A. DOUCET, AND A. JASRA, *Sequential Monte Carlo Samplers*, J. R. Stat. Soc. B, 68 (2006), pp. 411–436.
- [12] A. DEMBO AND O. ZEITOUNI, *Large Deviations Techniques and Applications*, vol. 38 of Stochastic Modelling and Applied Probability, Springer, Berlin, Heidelberg, 2010.

- [13] Z. DING AND Q. LI, *Ensemble Kalman inversion: Mean-field limit and convergence analysis*, Stat. Comput., 31 (2021), p. 9.
- [14] Z. DING AND Q. LI, *Ensemble Kalman Sampler: Mean-field Limit and Convergence Analysis*, SIAM J. Math. Anal., 53 (2021), pp. 1546–1578.
- [15] T. J. DODWELL, C. KETELSEN, R. SCHEICHL, AND A. L. TECKENTRUP, *A Hierarchical Multilevel Markov Chain Monte Carlo Algorithm with Applications to Uncertainty Quantification in Subsurface Flow*, SIAM/ASA J. Uncertainty Quantif., 3 (2015), pp. 1075–1108.
- [16] O. R. A. DUNBAR, A. B. DUNCAN, A. M. STUART, AND M.-T. WOLFRAM, *Ensemble Inference Methods for Models With Noisy and Expensive Likelihoods*, SIAM J. Appl. Dyn. Syst., 21 (2022), pp. 1539–1572.
- [17] G. EVENSEN, *Sequential data assimilation with a nonlinear quasi-geostrophic model using Monte Carlo methods to forecast error statistics*, J. Geophys. Res. Oceans, 99 (1994), pp. 10143–10162.
- [18] M. FORNASIER, T. KLOCK, AND K. RIEDL, *Consensus-Based Optimization Methods Converge Globally*, SIAM J. Optim., 34 (2024), pp. 2973–3004.
- [19] A. GARBUNO-INIGO, F. HOFFMANN, W. LI, AND A. M. STUART, *Interacting Langevin Diffusions: Gradient Structure and Ensemble Kalman Sampler*, SIAM J. Appl. Dyn. Syst., 19 (2020), pp. 412–441.
- [20] A. GARBUNO-INIGO, N. NÜSKEN, AND S. REICH, *Affine Invariant Interacting Langevin Dynamics for Bayesian Inference*, SIAM J. Appl. Dyn. Syst., 19 (2020), pp. 1633–1658.
- [21] N. J. GERBER, F. HOFFMANN, AND U. VAES, *Mean-field limits for Consensus-Based Optimization and Sampling*, arXiv:2312.07373, (2024).
- [22] J. GOODMAN AND J. WEARE, *Ensemble samplers with affine invariance*, Commun. Appl. Math. Comput. Sci., 5 (2010), pp. 65–80.
- [23] P. GREENGARD, *An ensembled Metropolized Langevin sampler*, Master’s thesis, Courant Institute, New York University, (2015).
- [24] W. K. HASTINGS, *Monte Carlo Sampling Methods Using Markov Chains and Their Applications*, Biometrika, 57 (1970), pp. 97–109.
- [25] L. HERRMANN, M. KELLER, AND C. SCHWAB, *Quasi-Monte Carlo Bayesian estimation under Besov priors in elliptic inverse problems*, Math. Comput., 90 (2021), pp. 1831–1860.
- [26] P. L. HOUTEKAMER AND H. L. MITCHELL, *Data Assimilation Using an Ensemble Kalman Filter Technique*, Mon. Weather Rev., 126 (1998), pp. 796–811.
- [27] D. Z. HUANG, T. SCHNEIDER, AND A. M. STUART, *Iterated Kalman methodology for inverse problems*, J. Comput. Phys., 463 (2022), p. 111262.
- [28] M. A. IGLESIAS, K. J. H. LAW, AND A. M. STUART, *Ensemble Kalman methods for inverse problems*, Inverse Probl., 29 (2013), p. 045001.
- [29] S. JIN, L. LI, AND J.-G. LIU, *Random Batch Methods (RBM) for interacting particle systems*, J. Comput. Phys., 400 (2020), p. 108877.

- [30] J. P. KAIPIO AND E. SOMERSALO, *Statistical and Computational Inverse Problems*, vol. 160 of Applied Mathematical Sciences, Springer, New York, NY, 2005.
- [31] M. KOSS, S. WEISSMANN, AND J. ZECH, *On the mean field limit of consensus based methods*, arXiv:2409.03518, (2024).
- [32] N. B. KOVACHKI AND A. M. STUART, *Ensemble Kalman inversion: A derivative-free technique for machine learning tasks*, *Inverse Probl.*, 35 (2019), p. 095005.
- [33] Y. T. LEE, R. SHEN, AND K. TIAN, *Structured Logconcave Sampling with a Restricted Gaussian Oracle*, in *Proceedings of Thirty Fourth Conference on Learning Theory*, PMLR, July 2021, pp. 2993–3050.
- [34] B. LEIMKUHLE, C. MATTHEWS, AND J. WEARE, *Ensemble preconditioning for Markov chain Monte Carlo simulation*, *Stat. Comput.*, 28 (2018), pp. 277–290.
- [35] M. B. LYKKEGAARD, T. J. DODWELL, C. FOX, G. MINGAS, AND R. SCHEICHL, *Multilevel Delayed Acceptance MCMC*, *SIAM/ASA J. Uncertainty Quantif.*, 11 (2023), pp. 1–30.
- [36] Y.-A. MA, T. CHEN, AND E. B. FOX, *A complete recipe for stochastic gradient MCMC*, in *Proceedings of the 28th International Conference on Neural Information Processing Systems - Volume 2*, NIPS’15, Cambridge, MA, USA, Dec. 2015, MIT Press, pp. 2917–2925.
- [37] N. METROPOLIS, A. W. ROSENBLUTH, M. N. ROSENBLUTH, A. H. TELLER, AND E. TELLER, *Equation of State Calculations by Fast Computing Machines*, *J. Chem. Phys.*, 21 (1953), pp. 1087–1092.
- [38] P. D. MILLER, *Applied Asymptotic Analysis*, vol. 75 of Graduate studies in mathematics, American Mathematical Soc., 2006.
- [39] M. MORZFELD, X. T. TONG, AND Y. M. MARZOUK, *Localization for MCMC: Sampling high-dimensional posterior distributions with local structure*, *J. Comput. Phys.*, 380 (2019), pp. 1–28.
- [40] N. NÜSKEN AND S. REICH, *Note on Interacting Langevin Diffusions: Gradient Structure and Ensemble Kalman Sampler by Garbuno-Inigo, Hoffmann, Li and Stuart*, arXiv:1908.10890, (2019).
- [41] S. OSHER, H. HEATON, AND S. WU FUNG, *A Hamilton-Jacobi-based proximal operator*, *Proc. Natl. Acad. Sci. U.S.A.*, 120 (2023), p. e2220469120.
- [42] E. OTT, B. R. HUNT, I. SZUNYOGH, A. V. ZIMIN, E. J. KOSTELICH, M. CORAZZA, E. KALNAY, D. PATIL, AND J. A. YORKE, *A local ensemble Kalman filter for atmospheric data assimilation*, *Tellus A: Dyn. Meteorol. Oceanogr.*, 56 (2004), pp. 415–428.
- [43] G. A. PAVLIOTIS, A. M. STUART, AND U. VAES, *Derivative-Free Bayesian Inversion Using Multiscale Dynamics*, *SIAM J. Appl. Dyn. Syst.*, 21 (2022), pp. 284–326.
- [44] M. PEREYRA, *Proximal Markov chain Monte Carlo algorithms*, *Stat. Comput.*, 26 (2016), pp. 745–760.
- [45] K. B. PETERSEN AND M. S. PEDERSEN, *The Matrix Cookbook*, 2006.

- [46] R. PINNAU, C. TOTZECK, O. TSE, AND S. MARTIN, *A consensus-based model for global optimization and its mean-field limit*, Math. Models Methods Appl. Sci., 27 (2017), pp. 183–204.
- [47] S. REICH AND S. WEISSMANN, *Fokker–Planck Particle Systems for Bayesian Inference: Computational Approaches*, SIAM/ASA J. Uncertainty Quantif., 9 (2021), pp. 446–482.
- [48] K. RIEDL, T. KLOCK, C. GELDHAUSER, AND M. FORNASIER, *Gradient is All You Need?*, arXiv:2306.09778, (2023).
- [49] G. O. ROBERTS AND R. L. TWEEDIE, *Exponential convergence of Langevin distributions and their discrete approximations*, Bernoulli, 2 (1996), pp. 341–363.
- [50] R. T. ROCKAFELLAR AND R. J. B. WETS, *Variational Analysis*, vol. 317 of Grundlehren der mathematischen Wissenschaften, Springer, Berlin, Heidelberg, 1998.
- [51] S. SÄRKKÄ AND A. SOLIN, *Applied Stochastic Differential Equations*, Institute of Mathematical Statistics Textbooks, Cambridge University Press, Cambridge, 2019.
- [52] C. SCHILLINGS AND A. M. STUART, *Analysis of the Ensemble Kalman Filter for Inverse Problems*, SIAM J. Numer. Anal., 55 (2017), pp. 1264–1290.
- [53] C. SCHILLINGS, C. TOTZECK, AND P. WACKER, *Ensemble-Based Gradient Inference for Particle Methods in Optimization and Sampling*, SIAM/ASA J. Uncertainty Quantif., 11 (2023), pp. 757–787.
- [54] L. SEELINGER, A. REINARZ, L. RANNABAUER, M. BADER, P. BASTIAN, AND R. SCHEICHL, *High performance uncertainty quantification with parallelized multilevel Markov chain Monte Carlo*, in Proceedings of the International Conference for High Performance Computing, Networking, Storage and Analysis, SC ’21, New York, NY, USA, Nov. 2021, Association for Computing Machinery, pp. 1–15.
- [55] A. M. STUART, *Inverse problems: A Bayesian perspective*, Acta Numer., 19 (2010), pp. 451–559.
- [56] A.-S. SZNITMAN, *Topics in propagation of chaos*, in Ecole d’Été de Probabilités de Saint-Flour XIX — 1989, D. L. Burkholder, E. Pardoux, A.-S. Sznitman, and P.-L. Hennequin, eds., Berlin, Heidelberg, 1991, Springer, pp. 165–251.
- [57] M. K. TITSIAS AND O. PAPASPILIOPOULOS, *Auxiliary Gradient-Based Sampling Algorithms*, J. R. Stat. Soc. B, 80 (2018), pp. 749–767.
- [58] X. T. TONG AND M. MORZFELD, *Localized ensemble kalman inversion*, Inverse Probl., 39 (2023), p. 064002.
- [59] P. WACKER, *Perspectives on locally weighted ensemble Kalman methods*, arXiv:2402.00027, (2024).
- [60] F. WAGNER, I. PAPAIOANNOU, AND E. ULLMANN, *The Ensemble Kalman Filter for Rare Event Estimation*, SIAM/ASA J. Uncertainty Quantif., 10 (2022), pp. 317–349.
- [61] S. YANG, Y. CHEN, E. BERNTON, AND J. S. LIU, *On parallelizable Markov chain Monte Carlo algorithms with waste-recycling*, Stat. Comput., 28 (2018), pp. 1073–1081.